

Tests of general relativity with GW150914

B. P. Abbott,¹ R. Abbott,¹ T. D. Abbott,² M. R. Abernathy,¹ F. Acernese,^{3,4} K. Ackley,⁵ C. Adams,⁶ T. Adams,⁷ P. Addesso,³ R. X. Adhikari,¹ V. B. Adya,⁸ C. Affeldt,⁸ M. Agathos,⁹ K. Agatsuma,⁹ N. Aggarwal,¹⁰ O. D. Aguiar,¹¹ L. Aiello,^{12,13} A. Ain,¹⁴ P. Ajith,¹⁵ B. Allen,^{8,16,17} A. Allocata,^{18,19} P. A. Altin,²⁰ S. B. Anderson,¹ W. G. Anderson,¹⁶ K. Arai,¹ M. C. Araya,¹ C. C. Arceneaux,²¹ J. S. Areeda,²² N. Arnaud,²³ K. G. Arun,²⁴ S. Ascenzi,^{25,13} G. Ashton,²⁶ M. Ast,²⁷ S. M. Aston,⁶ P. Astone,²⁸ P. Aufmuth,⁸ C. Aulbert,⁸ S. Babak,²⁹ P. Bacon,³⁰ M. K. M. Bader,⁹ P. T. Baker,³¹ F. Baldaccini,^{32,33} G. Ballardin,³⁴ S. W. Ballmer,³⁵ J. C. Barayoga,¹ S. E. Barclay,³⁶ B. C. Barish,¹ D. Barker,³⁷ F. Barone,^{3,4} B. Barr,³⁶ L. Barsotti,¹⁰ M. Barsuglia,³⁰ D. Barta,³⁸ J. Bartlett,³⁷ I. Bartos,³⁹ R. Bassiri,⁴⁰ A. Basti,^{18,19} J. C. Batch,³⁷ C. Baune,⁸ V. Bavigadda,³⁴ M. Bazzan,^{41,42} B. Behnke,²⁹ M. Bejger,⁴³ A. S. Bell,³⁶ C. J. Bell,³⁶ B. K. Berger,¹ J. Bergman,³⁷ G. Bergmann,⁸ C. P. L. Berry,⁴⁴ D. Bersanetti,^{45,46} A. Bertolini,⁹ J. Betzwieser,⁶ S. Bhagwat,³⁵ R. Bhandare,⁴⁷ I. A. Bilenko,⁴⁸ G. Billingsley,¹ J. Birch,⁶ R. Birney,⁴⁹ O. Birnholtz,⁸ S. Biscans,¹⁰ A. Bisht,^{8,17} M. Bitossi,³⁴ C. Biwer,³⁵ M. A. Bizouard,²³ J. K. Blackburn,¹ C. D. Blair,⁵⁰ D. G. Blair,⁵⁰ R. M. Blair,³⁷ S. Bloemen,⁵¹ O. Bock,⁸ T. P. Bodiya,¹⁰ M. Boer,⁵² G. Bogaert,⁵² C. Bogan,⁸ A. Bohe,²⁹ P. Bojtos,⁵³ C. Bond,⁴⁴ F. Bondi,⁵⁴ R. Bonnand,⁷ B. A. Boom,⁹ R. Bork,¹ V. Boschi,^{18,19} S. Bose,^{55,14} Y. Bouffanais,³⁰ A. Bozzi,³⁴ C. Bradaschia,¹⁹ P. R. Brady,¹⁶ V. B. Braginsky,⁴⁸ M. Branchesi,^{57,58} J. E. Brau,⁵⁹ T. Briant,⁶⁰ A. Brillet,⁵² M. Brinkmann,⁸ V. Brisson,²³ P. Brockill,¹⁶ A. F. Brooks,¹ D. A. Brown,³⁵ D. D. Brown,⁴⁴ N. M. Brown,¹⁰ C. C. Buchanan,² A. Buikema,¹⁰ T. Bulik,⁶¹ H. J. Bulten,^{62,9} A. Buonanno,^{29,63} D. Buskulic,⁷ C. Buy,³⁰ R. L. Byer,⁴⁰ L. Cadonati,⁶⁴ G. Cagnoli,^{65,66} C. Cahillane,¹ J. Calderón Bustillo,^{67,64} T. Callister,¹ E. Calloni,^{68,4} J. B. Camp,⁶⁹ K. C. Cannon,⁷⁰ J. Cao,⁷¹ C. D. Capano,⁸ E. Capocasa,³⁰ F. Carbognani,³⁴ S. Caride,⁷² J. Casanueva Diaz,²³ C. Casentini,^{25,13} S. Caudill,¹⁶ M. Cavaglià,²¹ F. Cavalier,²³ R. Cavalieri,³⁴ G. Cella,¹⁹ C. B. Cepeda,¹ L. Cerboni Baiardi,^{57,58} G. Cerretani,^{18,19} E. Cesarini,^{25,13} R. Chakraborty,¹ T. Chalermongsak,¹ S. J. Chamberlin,⁷³ M. Chan,³⁶ S. Chao,⁷⁴ P. Charlton,⁷⁵ E. Chassande-Mottin,³⁰ H. Y. Chen,⁷⁶ Y. Chen,⁷⁷ C. Cheng,⁷⁴ A. Chincarini,⁴⁶ A. Chiummo,³⁴ H. S. Cho,⁷⁸ M. Cho,⁶³ J. H. Chow,²⁰ N. Christensen,⁷⁹ Q. Chu,⁵⁰ S. Chua,⁶⁰ S. Chung,⁵⁰ G. Ciani,⁵ F. Clara,³⁷ J. A. Clark,⁶⁴ F. Cleva,⁵² E. Coccia,^{25,12,13} P.-F. Cohadon,⁶⁰ A. Colla,^{80,28} C. G. Collette,⁸¹ L. Cominsky,⁸² M. Constancio Jr.,¹¹ A. Conte,^{80,28} L. Conti,⁴² D. Cook,³⁷ T. R. Corbitt,² N. Cornish,³¹ A. Corsi,⁷² S. Cortese,³⁴ C. A. Costa,¹¹ M. W. Coughlin,⁷⁹ S. B. Coughlin,⁸³ J.-P. Coulon,⁵² S. T. Countryman,³⁹ P. Couvares,¹ E. E. Cowan,⁶⁴ D. M. Coward,⁵⁰ M. J. Cowart,⁶ D. C. Coyne,¹ R. Coyne,⁷² K. Craig,³⁶ J. D. E. Creighton,¹⁶ J. Cripe,² S. G. Crowder,⁸⁴ A. Cumming,³⁶ L. Cunningham,³⁶ E. Cuoco,³⁴ T. Dal Canton,⁸ S. L. Danilishin,³⁶ S. D'Antonio,¹³ K. Danzmann,^{17,8} N. S. Darman,⁸⁵ V. Dattilo,³⁴ I. Dave,⁴⁷ H. P. Daveloza,⁸⁶ M. Davier,²³ G. S. Davies,³⁶ E. J. Daw,⁸⁷ R. Day,³⁴ D. DeBra,⁴⁰ G. Debreczeni,³⁸ J. Degallaix,⁶⁶ M. De Laurentis,^{68,4} S. Deléglise,⁶⁰ W. Del Pozzo,⁴⁴ T. Denker,^{8,17} T. Dent,⁸ H. Dereli,⁵² V. Dergachev,¹ R. De Rosa,^{68,4} R. T. DeRosa,⁶ R. DeSalvo,⁸⁸ S. Dhurandhar,¹⁴ M. C. Díaz,⁸⁶ L. Di Fiore,⁴ M. Di Giovanni,^{80,28} A. Di Lieto,^{18,19} S. Di Pace,^{80,28} I. Di Palma,^{29,8} A. Di Virgilio,¹⁹ G. Dojcinoski,⁸⁹ V. Dolique,⁶⁶ F. Donovan,¹⁰ K. L. Dooley,²¹ S. Doravari,^{6,8} R. Douglas,³⁶ T. P. Downes,¹⁶ M. Drago,^{8,90,91} R. W. P. Drever,¹ J. C. Driggers,³⁷ Z. Du,⁷¹ M. Ducrot,⁷ S. E. Dwyer,³⁷ T. B. Edo,⁸⁷ M. C. Edwards,⁷⁹ A. Effler,⁶ H.-B. Eggenstein,⁸ P. Ehrens,¹ J. Eichholz,⁵ S. S. Eikenberry,⁵ W. Engels,⁷⁷ R. C. Essick,¹⁰ T. Etzel,¹ M. Evans,¹⁰ T. M. Evans,⁶ R. Everett,⁷³ M. Factourovich,³⁹ V. Fafone,^{25,13,12} H. Fair,³⁵ S. Fairhurst,⁹² X. Fan,⁷¹ Q. Fang,⁵⁰ S. Farinon,⁴⁶ B. Farr,⁷⁶ W. M. Farr,⁴⁴ M. Favata,⁸⁹ M. Fays,⁹² H. Fehrmann,⁸ M. M. Fejer,⁴⁰ I. Ferrante,^{18,19} E. C. Ferreira,¹¹ F. Ferrini,³⁴ F. Fidecaro,^{18,19} I. Fiori,³⁴ D. Fiorucci,³⁰ R. P. Fisher,³⁵ R. Flaminio,^{66,93} M. Fletcher,³⁶ J.-D. Fournier,⁵² S. Franco,²³ S. Frasca,^{80,28} F. Frasconi,¹⁹ Z. Frei,⁵³ A. Freise,⁴⁴ R. Frey,⁵⁹ V. Frey,²³ T. T. Fricke,⁸ P. Fritschel,¹⁰ V. V. Frolov,⁶ P. Fulda,⁵ M. Fyffe,⁶ H. A. G. Gabbard,²¹ J. R. Gair,⁹⁴ L. Gammaioni,^{32,33} S. G. Gaonkar,¹⁴ F. Garufi,^{68,4} A. Gatto,³⁰ G. Gaur,^{95,96} N. Gehrels,⁶⁹ G. Gemme,⁴⁶ B. Gendre,⁵² E. Genin,³⁴ A. Gennai,¹⁹ J. George,⁴⁷ L. Gergely,⁹⁷ V. Germain,⁷ Abhirup Ghosh,¹⁵ Archisman Ghosh,¹⁵ S. Ghosh,^{51,9} J. A. Giaime,^{2,6} K. D. Giardina,⁶ A. Giazotto,¹⁹ K. Gill,⁹⁸ A. Glaefke,³⁶ E. Goetz,⁹⁹ R. Goetz,⁵ L. Gondan,⁵³ G. González,² J. M. Gonzalez Castro,^{18,19} A. Gopakumar,¹⁰⁰ N. A. Gordon,³⁶ M. L. Gorodetsky,⁴⁸ S. E. Gossan,¹ M. Gosselin,³⁴ R. Gouaty,⁷ C. Graef,³⁶ P. B. Graff,⁶³ M. Granata,⁶⁶ A. Grant,³⁶ S. Gras,¹⁰ C. Gray,³⁷ G. Greco,^{57,58} A. C. Green,⁴⁴ P. Groot,⁵¹ H. Grote,⁸ S. Grunewald,²⁹ G. M. Guidi,^{57,58} X. Guo,⁷¹ A. Gupta,¹⁴ M. K. Gupta,⁹⁶ K. E. Gushwa,¹ E. K. Gustafson,¹ R. Gustafson,⁹⁹ J. J. Hacker,²² B. R. Hall,⁵⁵ E. D. Hall,¹ G. Hammond,³⁶ M. Haney,¹⁰⁰ M. M. Hanke,⁸ J. Hanks,³⁷ C. Hanna,⁷³ M. D. Hannam,⁹² J. Hanson,⁶ T. Hardwick,² J. Harms,^{57,58} G. M. Harry,¹⁰¹ I. W. Harry,²⁹ M. J. Hart,³⁶ M. T. Hartman,⁵ C.-J. Haster,⁴⁴ K. Haughian,³⁶ J. Healy,¹⁰² A. Heidmann,⁶⁰ M. C. Heintze,^{5,6} H. Heitmann,⁵² P. Hello,²³ G. Hemming,³⁴ M. Hendry,³⁶ I. S. Heng,³⁶ J. Hennig,³⁶ A. W. Heptonstall,¹ M. Heurs,^{8,17} S. Hild,³⁶ D. Hoak,¹⁰³ K. A. Hodge,¹ D. Hoffman,⁶⁶ S. E. Hollitt,¹⁰⁴ K. Holt,⁶ D. E. Holz,⁷⁶ P. Hopkins,⁹² D. J. Hosken,¹⁰⁴ J. Hough,³⁶ E. A. Houston,³⁶ E. J. Howell,⁵⁰ Y. M. Hu,³⁶ S. Huang,⁷⁴ E. A. Huerta,^{105,83} D. Huet,²³ B. Hughey,⁹⁸ S. Husa,⁶⁷ S. H. Huttner,³⁶ T. Huynh-Dinh,⁶ A. Idrisy,⁷³ N. Indik,⁸ D. R. Ingram,³⁷ R. Inta,⁷² H. N. Isa,³⁶ J.-M. Isac,⁶⁰ M. Isi,¹ G. Islas,²² T. Isogai,¹⁰ B. R. Iyer,¹⁵ K. Izumi,³⁷ T. Jacqmin,⁶⁰ H. Jang,⁷⁸ K. Jani,⁶⁴ P. Jaranowski,¹⁰⁶ S. Jawahar,¹⁰⁷

F. Jiménez-Forteza,⁶⁷ W. W. Johnson,² N. K. Johnson-McDaniel,¹⁵ D. I. Jones,²⁶ R. Jones,³⁶ R. J. G. Jonker,⁹ L. Ju,⁵⁰ Haris K,¹⁰⁸ C. V. Kalaghpatgi,^{24,92} V. Kalogera,⁸³ S. Kandhasamy,²¹ G. Kang,⁷⁸ J. B. Kanner,¹ S. Karki,⁵⁹ M. Kasprzack,^{2,23,34} E. Katsavounidis,¹⁰ W. Katzman,⁶ S. Kaufer,¹⁷ T. Kaur,⁵⁰ K. Kawabe,³⁷ F. Kawazoe,^{8,17} F. Kéfélian,⁵² M. S. Kehl,⁷⁰ D. Keitel,^{8,67} D. B. Kelley,³⁵ W. Kells,¹ R. Kennedy,⁸⁷ J. S. Key,⁸⁶ A. Khalaïdovski,⁸ F. Y. Khalili,⁴⁸ I. Khan,¹² S. Khan,⁹² Z. Khan,⁹⁶ E. A. Khazanov,¹⁰⁹ N. Kijbunchoo,³⁷ C. Kim,⁷⁸ J. Kim,¹¹⁰ K. Kim,¹¹¹ Nam-Gyu Kim,⁷⁸ Namjun Kim,⁴⁰ Y.-M. Kim,¹¹⁰ E. J. King,¹⁰⁴ P. J. King,³⁷ D. L. Kinzel,⁶ J. S. Kissel,³⁷ L. Kleybolte,²⁷ S. Klimenko,⁵ S. M. Koehlenbeck,⁸ K. Kokeyama,² S. Koley,⁹ V. Kondrashov,¹ A. Kontos,¹⁰ M. Korobko,²⁷ W. Z. Korth,¹ I. Kowalska,⁶¹ D. B. Kozak,¹ V. Kringel,⁸ B. Krishnan,⁸ A. Królak,^{112,113} C. Krueger,¹⁷ G. Kuehn,⁸ P. Kumar,⁷⁰ L. Kuo,⁷⁴ A. Kutynia,¹¹² B. D. Lackey,³⁵ M. Landry,³⁷ J. Lange,¹⁰² B. Lantz,⁴⁰ P. D. Lasky,¹¹⁴ A. Lazzarini,¹ C. Lazzaro,^{64,42} P. Leaci,^{29,80,28} S. Leavey,³⁶ E. O. Lebigot,^{30,71} C. H. Lee,¹¹⁰ H. K. Lee,¹¹¹ H. M. Lee,¹¹⁵ K. Lee,³⁶ A. Lenon,³⁵ M. Leonardi,^{90,91} J. R. Leong,⁸ N. Leroy,²³ N. Letendre,⁷ Y. Levin,¹¹⁴ B. M. Levine,³⁷ T. G. F. Li,¹ A. Libson,¹⁰ T. B. Littenberg,¹¹⁶ N. A. Lockerbie,¹⁰⁷ J. Logue,³⁶ A. L. Lombardi,¹⁰³ L. T. London,⁹² J. E. Lord,³⁵ M. Lorenzini,^{12,13} V. Loriette,¹¹⁷ M. Lormand,⁶ G. Losurdo,⁵⁸ J. D. Lough,^{8,17} C. O. Lousto,¹⁰² G. Lovelace,²² H. Lück,^{17,8} A. P. Lundgren,⁸ J. Luo,⁷⁹ R. Lynch,¹⁰ Y. Ma,⁵⁰ T. MacDonald,⁴⁰ B. Machenschalk,⁸ M. MacInnis,¹⁰ D. M. Macleod,² F. Magaña-Sandoval,³⁵ R. M. Magee,⁵⁵ M. Mageswaran,¹ E. Majorana,²⁸ I. Maksimovic,¹¹⁷ V. Malvezzi,^{25,13} N. Man,⁵² I. Mandel,⁴⁴ V. Mandic,⁸⁴ V. Mangano,³⁶ G. L. Mansell,²⁰ M. Manske,¹⁶ M. Mantovani,³⁴ F. Marchesoni,^{118,33} F. Marion,⁷ S. Márka,³⁹ Z. Márka,³⁹ A. S. Markosyan,⁴⁰ E. Maros,¹ F. Martelli,^{57,58} L. Martellini,⁵² I. W. Martin,³⁶ R. M. Martin,⁵ D. V. Martynov,¹ J. N. Marx,¹ K. Mason,¹⁰ A. Masserot,⁷ T. J. Massinger,³⁵ M. Masso-Reid,³⁶ F. Matichard,¹⁰ L. Matone,³⁹ N. Mavalvala,¹⁰ N. Mazumder,⁵⁵ G. Mazzolo,⁸ R. McCarthy,³⁷ D. E. McClelland,²⁰ S. McCormick,⁶ S. C. McGuire,¹¹⁹ G. McIntyre,¹ J. McIver,¹ D. J. McManus,²⁰ S. T. McWilliams,¹⁰⁵ D. Meacher,⁷³ G. D. Meadors,^{29,8} J. Meidam,⁹ A. Melatos,⁸⁵ G. Mendell,³⁷ D. Mendoza-Gandara,⁸ R. A. Mercer,¹⁶ E. Merilh,³⁷ M. Merzougui,⁵² S. Meshkov,¹ C. Messenger,³⁶ C. Messick,⁷³ P. M. Meyers,⁸⁴ F. Mezzani,^{28,80} H. Miao,⁴⁴ C. Michel,⁶⁶ H. Middleton,⁴⁴ E. E. Mikhailov,¹²⁰ L. Milano,^{68,4} J. Miller,¹⁰ M. Millhouse,³¹ Y. Minenkov,¹³ J. Ming,^{29,8} S. Mirshekari,¹²¹ C. Mishra,¹⁵ S. Mitra,¹⁴ V. P. Mitrofanov,⁴⁸ G. Mitselmakher,⁵ R. Mittelman,¹⁰ A. Moggi,¹⁹ M. Mohan,³⁴ S. R. P. Mohapatra,¹⁰ M. Montani,^{57,58} B. C. Moore,⁸⁹ C. J. Moore,¹²² D. Moraru,³⁷ G. Moreno,³⁷ S. R. Morris,⁸⁶ K. Mossavi,⁸ B. Mours,⁷ C. M. Mow-Lowry,⁴⁴ C. L. Mueller,⁵ G. Mueller,⁵ A. W. Muir,⁹² Arunava Mukherjee,¹⁵ D. Mukherjee,¹⁶ S. Mukherjee,⁸⁶ N. Mukund,¹⁴ A. Mullavey,⁶ J. Munch,¹⁰⁴ D. J. Murphy,³⁹ P. G. Murray,³⁶ A. Mytidis,⁵ I. Nardcchia,^{25,13} L. Naticchioni,^{80,28} R. K. Nayak,¹²³ V. Necula,⁵ K. Nedkova,¹⁰³ G. Nelemans,^{51,9} M. Neri,^{45,46} A. Neunzert,⁹⁹ G. Newton,³⁶ T. T. Nguyen,²⁰ A. B. Nielsen,⁸ S. Nissanké,^{51,9} A. Nitz,⁸ F. Nocera,³⁴ D. Nolting,⁶ M. E. Normandin,⁸⁶ L. K. Nuttall,³⁵ J. Oberling,³⁷ E. Ochsner,¹⁶ J. O'Dell,¹²⁴ E. Oelker,¹⁰ G. H. Ogin,¹²⁵ J. J. Oh,¹²⁶ S. H. Oh,¹²⁶ F. Ohme,⁹² M. Oliver,⁶⁷ P. Oppermann,⁸ Richard J. Oram,⁶ B. O'Reilly,⁶ R. O'Shaughnessy,¹⁰² D. J. Ottaway,¹⁰⁴ R. S. Ottens,⁵ H. Overmier,⁶ B. J. Owen,⁷² A. Pai,¹⁰⁸ S. A. Pai,⁴⁷ J. R. Palamos,⁵⁹ O. Palashov,¹⁰⁹ C. Palomba,²⁸ A. Pal-Singh,²⁷ H. Pan,⁷⁴ Y. Pan,⁶³ C. Pankow,⁸³ F. Pannarale,⁹² B. C. Pant,⁴⁷ F. Paoletti,^{34,19} A. Paoli,³⁴ M. A. Papa,^{29,16,8} H. R. Paris,⁴⁰ W. Parker,⁶ D. Pascucci,³⁶ A. Pasqualetti,³⁴ R. Passaquieti,^{18,19} D. Passuello,¹⁹ B. Patricelli,^{18,19} Z. Patrick,⁴⁰ B. L. Pearlstone,³⁶ M. Pedraza,¹ R. Pedurand,⁶⁶ L. Pekowsky,³⁵ A. Pele,⁶ S. Penn,¹²⁷ A. Perreca,¹ H. P. Pfeiffer,^{70,29} M. Phelps,³⁶ O. Piccinni,^{80,28} M. Pichot,⁵² F. Piergiovanni,^{57,58} V. Pierro,⁸⁸ G. Pillant,³⁴ L. Pinard,⁶⁶ I. M. Pinto,⁸⁸ M. Pitkin,³⁶ R. Poggiani,^{18,19} P. Popolizio,³⁴ A. Post,⁸ J. Powell,³⁶ J. Prasad,¹⁴ V. Predoi,⁹² S. S. Premachandra,¹¹⁴ T. Prestegard,⁸⁴ L. R. Price,¹ M. Prijatelj,³⁴ M. Principe,⁸⁸ S. Privitera,²⁹ R. Prix,⁸ G. A. Prodi,^{90,91} L. Prokhorov,⁴⁸ O. Puncken,⁸ M. Punturo,³³ P. Puppo,²⁸ M. Pürer,²⁹ H. Qi,¹⁶ J. Qin,⁵⁰ V. Quetschke,⁸⁶ E. A. Quintero,¹ R. Quitzow-James,⁵⁹ F. J. Raab,³⁷ D. S. Rabeling,²⁰ H. Radkins,³⁷ P. Raffai,⁵³ S. Raja,⁴⁷ M. Rakhmanov,⁸⁶ P. Rapagnani,^{80,28} V. Raymond,²⁹ M. Razzano,^{18,19} V. Re,²⁵ J. Read,²² C. M. Reed,³⁷ T. Regimbau,⁵² L. Rei,⁴⁶ S. Reid,⁴⁹ D. H. Reitze,^{1,5} H. Rew,¹²⁰ S. D. Reyes,³⁵ F. Ricci,^{80,28} K. Riles,⁹⁹ N. A. Robertson,^{1,36} R. Robie,³⁶ F. Robinet,²³ A. Rocchi,¹³ L. Rolland,⁷ J. G. Rollins,¹ V. J. Roma,⁵⁹ R. Romano,^{3,4} G. Romanov,¹²⁰ J. H. Romie,⁶ D. Rosińska,^{128,43} S. Rowan,³⁶ A. Rüdiger,⁸ P. Ruggi,³⁴ K. Ryan,³⁷ S. Sachdev,¹ T. Sadecki,³⁷ L. Sadeghian,¹⁶ L. Salconi,³⁴ M. Saleem,¹⁰⁸ F. Salemi,⁸ A. Samajdar,¹²³ L. Sammut,^{85,114} E. J. Sanchez,¹ V. Sandberg,³⁷ B. Sandeen,⁸³ J. R. Sanders,^{99,35} B. Sassolas,⁶⁶ B. S. Sathyaprakash,⁹² P. R. Saulson,³⁵ O. Sauter,⁹⁹ R. L. Savage,³⁷ A. Sawadsky,¹⁷ P. Schale,⁵⁹ R. Schilling,⁸ J. Schmidt,⁸ P. Schmidt,^{1,77} R. Schnabel,²⁷ R. M. S. Schofield,⁵⁹ A. Schönbeck,²⁷ E. Schreiber,⁸ D. Schuette,^{8,17} B. F. Schutz,^{92,29} J. Scott,³⁶ S. M. Scott,²⁰ D. Sellers,⁶ A. S. Sengupta,⁹⁵ D. Sentenac,³⁴ V. Sequino,^{25,13} A. Sergeev,¹⁰⁹ G. Serna,²² Y. Setyawati,^{51,9} A. Sevigny,³⁷ D. A. Shaddock,²⁰ S. Shah,^{51,9} M. S. Shahriar,⁸³ M. Shaltev,⁸ Z. Shao,¹ B. Shapiro,⁴⁰ P. Shawhan,⁶³ A. Sheperd,¹⁶ D. H. Shoemaker,¹⁰ D. M. Shoemaker,⁶⁴ K. Siellez,^{52,64} X. Siemens,¹⁶ D. Sigg,³⁷ A. D. Silva,¹¹ D. Simakov,⁸ A. Singer,¹ L. P. Singer,⁶⁹ A. Singh,^{29,8} R. Singh,² A. Singhal,¹² A. M. Sintes,⁶⁷ B. J. J. Slagmolen,²⁰ J. R. Smith,²² N. D. Smith,¹ R. J. E. Smith,¹ E. J. Son,¹²⁶ B. Sorazu,³⁶ F. Sorrentino,⁴⁶ T. Souradeep,¹⁴ A. K. Srivastava,⁹⁶ A. Staley,³⁹ M. Steinke,⁸ J. Steinlechner,³⁶ S. Steinlechner,³⁶ D. Steinmeyer,^{8,17} B. C. Stephens,¹⁶

R. Stone,⁸⁶ K. A. Strain,³⁶ N. Straniero,⁶⁶ G. Stratta,^{57,58} N. A. Strauss,⁷⁹ S. Strigin,⁴⁸ R. Sturani,¹²¹ A. L. Stuver,⁶ T. Z. Summerscales,¹²⁹ L. Sun,⁸⁵ P. J. Sutton,⁹² B. L. Swinkels,³⁴ M. J. Szczepańczyk,⁹⁸ M. Tacca,³⁰ D. Talukder,⁵⁹ D. B. Tanner,⁵ M. Tápai,⁹⁷ S. P. Tarabrin,⁸ A. Taracchini,²⁹ R. Taylor,¹ T. Theeg,⁸ M. P. Thirugnanasambandam,¹ E. G. Thomas,⁴⁴ M. Thomas,⁶ P. Thomas,³⁷ K. A. Thorne,⁶ K. S. Thorne,⁷⁷ E. Thrane,¹¹⁴ S. Tiwari,¹² V. Tiwari,⁹² K. V. Tokmakov,¹⁰⁷ C. Tomlinson,⁸⁷ M. Tonelli,^{18,19} C. V. Torres,^{‡,86} C. I. Torrie,¹ D. Töyrä,⁴⁴ F. Travasso,^{32,33} G. Traylor,⁶ D. Trifirò,²¹ M. C. Tringali,^{90,91} L. Trozzo,^{131,19} M. Tse,¹⁰ M. Turconi,⁵² D. Tuyenbayev,⁸⁶ D. Ugolini,¹³² C. S. Unnikrishnan,¹⁰⁰ A. L. Urban,¹⁶ S. A. Usman,³⁵ H. Vahlbruch,¹⁷ G. Vajente,¹ G. Valdes,⁸⁶ M. Vallisneri,⁷⁷ N. van Bakel,⁹ M. van Beuzekom,⁹ J. F. J. van den Brand,^{62,9} C. Van Den Broeck,⁹ D. C. Vander-Hyde,^{35,22} L. van der Schaaf,⁹ J. V. van Heijningen,⁹ A. A. van Veggel,³⁶ M. Vardaro,^{41,42} S. Vass,¹ M. Vasúth,³⁸ R. Vaulin,¹⁰ A. Vecchio,⁴⁴ G. Vedovato,⁴² J. Veitch,⁴⁴ P. J. Veitch,¹⁰⁴ K. Venkateswara,¹³³ D. Verkindt,⁷ F. Vetrano,^{57,58} A. Viceré,^{57,58} S. Vinciguerra,⁴⁴ D. J. Vine,⁴⁹ J.-Y. Vinet,⁵² S. Vitale,¹⁰ T. Vo,³⁵ H. Vocca,^{32,33} C. Vorvick,³⁷ D. Voss,⁵ W. D. Vousden,⁴⁴ S. P. Vyatchanin,⁴⁸ A. R. Wade,²⁰ L. E. Wade,¹³⁴ M. Wade,¹³⁴ M. Walker,² L. Wallace,¹ S. Walsh,^{16,8,29} G. Wang,¹² H. Wang,⁴⁴ M. Wang,⁴⁴ X. Wang,⁷¹ Y. Wang,⁵⁰ R. L. Ward,²⁰ J. Warner,³⁷ M. Was,⁷ B. Weaver,³⁷ L.-W. Wei,⁵² M. Weinert,⁸ A. J. Weinstein,¹ R. Weiss,¹⁰ T. Welborn,⁶ L. Wen,⁵⁰ P. Weßels,⁸ T. Westphal,⁸ K. Wette,⁸ J. T. Whelan,^{102,8} D. J. White,⁸⁷ B. F. Whiting,⁵ D. Williams,³⁶ R. D. Williams,¹ A. R. Williamson,⁹² J. L. Willis,¹³⁵ B. Willke,^{17,8} M. H. Wimmer,^{8,17} W. Winkler,⁸ C. C. Wipf,¹ H. Wittel,^{8,17} G. Woan,³⁶ J. Worden,³⁷ J. L. Wright,³⁶ G. Wu,⁶ J. Yablon,⁸³ W. Yam,¹⁰ H. Yamamoto,¹ C. C. Yancey,⁶³ M. J. Yap,²⁰ H. Yu,¹⁰ M. Yvert,⁷ A. Zadrożny,¹¹² L. Zangrandi,⁴² M. Zanolini,⁹⁸ J.-P. Zendri,⁴² M. Zevin,⁸³ F. Zhang,¹⁰ L. Zhang,¹ M. Zhang,¹²⁰ Y. Zhang,¹⁰² C. Zhao,⁵⁰ M. Zhou,⁸³ Z. Zhou,⁸³ X. J. Zhu,⁵⁰ M. E. Zucker,^{1,10} S. E. Zuraw,¹⁰³ and J. Zweizig¹

(LIGO Scientific Collaboration and Virgo Collaboration)

M. Boyle,⁵⁶ M. Campanelli,¹⁰² D. A. Hemberger,⁷⁷ L. E. Kidder,⁵⁶
 S. Ossokine,²⁹ M. A. Scheel,⁷⁷ B. Szilagyi,^{77,130} S. Teukolsky,⁵⁶
 and Y. Zlochower¹⁰²

[†]Deceased, May 2015. [‡]Deceased, March 2015.

¹LIGO, California Institute of Technology, Pasadena, CA 91125, USA

²Louisiana State University, Baton Rouge, LA 70803, USA

³Università di Salerno, Fisciano, I-84084 Salerno, Italy

⁴INFN, Sezione di Napoli, Complesso Universitario di Monte S. Angelo, I-80126 Napoli, Italy

⁵University of Florida, Gainesville, FL 32611, USA

⁶LIGO Livingston Observatory, Livingston, LA 70754, USA

⁷Laboratoire d'Annecy-le-Vieux de Physique des Particules (LAPP),

Université Savoie Mont Blanc, CNRS/IN2P3, F-74941 Annecy-le-Vieux, France

⁸Albert-Einstein-Institut, Max-Planck-Institut für Gravitationsphysik, D-30167 Hannover, Germany

⁹Nikhef, Science Park, 1098 XG Amsterdam, Netherlands

¹⁰LIGO, Massachusetts Institute of Technology, Cambridge, MA 02139, USA

¹¹Instituto Nacional de Pesquisas Espaciais, 12227-010 São José dos Campos, São Paulo, Brazil

¹²INFN, Gran Sasso Science Institute, I-67100 L'Aquila, Italy

¹³INFN, Sezione di Roma Tor Vergata, I-00133 Roma, Italy

¹⁴Inter-University Centre for Astronomy and Astrophysics, Pune 411007, India

¹⁵International Centre for Theoretical Sciences, Tata Institute of Fundamental Research, Bangalore 560012, India

¹⁶University of Wisconsin-Milwaukee, Milwaukee, WI 53201, USA

¹⁷Leibniz Universität Hannover, D-30167 Hannover, Germany

¹⁸Università di Pisa, I-56127 Pisa, Italy

¹⁹INFN, Sezione di Pisa, I-56127 Pisa, Italy

²⁰Australian National University, Canberra, Australian Capital Territory 0200, Australia

²¹The University of Mississippi, University, MS 38677, USA

²²California State University Fullerton, Fullerton, CA 92831, USA

²³LAL, Université Paris-Sud, CNRS/IN2P3, Université Paris-Saclay, 91400 Orsay, France

²⁴Chennai Mathematical Institute, Chennai 603103, India

²⁵Università di Roma Tor Vergata, I-00133 Roma, Italy

²⁶University of Southampton, Southampton SO17 1BJ, United Kingdom

²⁷Universität Hamburg, D-22761 Hamburg, Germany

²⁸INFN, Sezione di Roma, I-00185 Roma, Italy

²⁹Albert-Einstein-Institut, Max-Planck-Institut für Gravitationsphysik, D-14476 Potsdam-Golm, Germany

³⁰APC, AstroParticule et Cosmologie, Université Paris Diderot, CNRS/IN2P3, CEA/Irfu,

Observatoire de Paris, Sorbonne Paris Cité, F-75205 Paris Cedex 13, France

³¹Montana State University, Bozeman, MT 59717, USA

³²*Università di Perugia, I-06123 Perugia, Italy*
³³*INFN, Sezione di Perugia, I-06123 Perugia, Italy*
³⁴*European Gravitational Observatory (EGO), I-56021 Cascina, Pisa, Italy*
³⁵*Syracuse University, Syracuse, NY 13244, USA*
³⁶*SUPA, University of Glasgow, Glasgow G12 8QQ, United Kingdom*
³⁷*LIGO Hanford Observatory, Richland, WA 99352, USA*
³⁸*Wigner RCP, RMKI, H-1121 Budapest, Konkoly Thege Miklós út 29-33, Hungary*
³⁹*Columbia University, New York, NY 10027, USA*
⁴⁰*Stanford University, Stanford, CA 94305, USA*
⁴¹*Università di Padova, Dipartimento di Fisica e Astronomia, I-35131 Padova, Italy*
⁴²*INFN, Sezione di Padova, I-35131 Padova, Italy*
⁴³*CAMK-PAN, 00-716 Warsaw, Poland*
⁴⁴*University of Birmingham, Birmingham B15 2TT, United Kingdom*
⁴⁵*Università degli Studi di Genova, I-16146 Genova, Italy*
⁴⁶*INFN, Sezione di Genova, I-16146 Genova, Italy*
⁴⁷*RRCAT, Indore MP 452013, India*
⁴⁸*Faculty of Physics, Lomonosov Moscow State University, Moscow 119991, Russia*
⁴⁹*SUPA, University of the West of Scotland, Paisley PA1 2BE, United Kingdom*
⁵⁰*University of Western Australia, Crawley, Western Australia 6009, Australia*
⁵¹*Department of Astrophysics/IMAPP, Radboud University Nijmegen, P.O. Box 9010, 6500 GL Nijmegen, Netherlands*
⁵²*Artemis, Université Côte d'Azur, CNRS, Observatoire Côte d'Azur, CS 34229, Nice cedex 4, France*
⁵³*MTA Eötvös University, "Lendulet" Astrophysics Research Group, Budapest 1117, Hungary*
⁵⁴*Institut de Physique de Rennes, CNRS, Université de Rennes 1, F-35042 Rennes, France*
⁵⁵*Washington State University, Pullman, WA 99164, USA*
⁵⁶*Cornell University, Ithaca, NY 14853, USA*
⁵⁷*Università degli Studi di Urbino "Carlo Bo," I-61029 Urbino, Italy*
⁵⁸*INFN, Sezione di Firenze, I-50019 Sesto Fiorentino, Firenze, Italy*
⁵⁹*University of Oregon, Eugene, OR 97403, USA*
⁶⁰*Laboratoire Kastler Brossel, UPMC-Sorbonne Universités, CNRS, ENS-PSL Research University, Collège de France, F-75005 Paris, France*
⁶¹*Astronomical Observatory Warsaw University, 00-478 Warsaw, Poland*
⁶²*VU University Amsterdam, 1081 HV Amsterdam, Netherlands*
⁶³*University of Maryland, College Park, MD 20742, USA*
⁶⁴*Center for Relativistic Astrophysics and School of Physics, Georgia Institute of Technology, Atlanta, GA 30332, USA*
⁶⁵*Institut Lumière Matière, Université de Lyon, Université Claude Bernard Lyon 1, UMR CNRS 5306, 69622 Villeurbanne, France*
⁶⁶*Laboratoire des Matériaux Avancés (LMA), IN2P3/CNRS, Université de Lyon, F-69622 Villeurbanne, Lyon, France*
⁶⁷*Universitat de les Illes Balears, IAC3—IEEC, E-07122 Palma de Mallorca, Spain*
⁶⁸*Università di Napoli "Federico II," Complesso Universitario di Monte S.Angelo, I-80126 Napoli, Italy*
⁶⁹*NASA/Goddard Space Flight Center, Greenbelt, MD 20771, USA*
⁷⁰*Canadian Institute for Theoretical Astrophysics, University of Toronto, Toronto, Ontario M5S 3H8, Canada*
⁷¹*Tsinghua University, Beijing 100084, China*
⁷²*Texas Tech University, Lubbock, TX 79409, USA*
⁷³*The Pennsylvania State University, University Park, PA 16802, USA*
⁷⁴*National Tsing Hua University, Hsinchu City, 30013 Taiwan, Republic of China*
⁷⁵*Charles Sturt University, Wagga Wagga, New South Wales 2678, Australia*
⁷⁶*University of Chicago, Chicago, IL 60637, USA*
⁷⁷*Caltech CaRT, Pasadena, CA 91125, USA*
⁷⁸*Korea Institute of Science and Technology Information, Daejeon 305-806, Korea*
⁷⁹*Carleton College, Northfield, MN 55057, USA*
⁸⁰*Università di Roma "La Sapienza," I-00185 Roma, Italy*
⁸¹*University of Brussels, Brussels 1050, Belgium*
⁸²*Sonoma State University, Rohnert Park, CA 94928, USA*
⁸³*Northwestern University, Evanston, IL 60208, USA*
⁸⁴*University of Minnesota, Minneapolis, MN 55455, USA*
⁸⁵*The University of Melbourne, Parkville, Victoria 3010, Australia*
⁸⁶*The University of Texas Rio Grande Valley, Brownsville, TX 78520, USA*
⁸⁷*The University of Sheffield, Sheffield S10 2TN, United Kingdom*
⁸⁸*University of Sannio at Benevento, I-82100 Benevento, Italy and INFN, Sezione di Napoli, I-80100 Napoli, Italy*
⁸⁹*Montclair State University, Montclair, NJ 07043, USA*
⁹⁰*Università di Trento, Dipartimento di Fisica, I-38123 Povo, Trento, Italy*
⁹¹*INFN, Trento Institute for Fundamental Physics and Applications, I-38123 Povo, Trento, Italy*

⁹²*Cardiff University, Cardiff CF24 3AA, United Kingdom*
⁹³*National Astronomical Observatory of Japan, 2-21-1 Osawa, Mitaka, Tokyo 181-8588, Japan*
⁹⁴*School of Mathematics, University of Edinburgh, Edinburgh EH9 3FD, United Kingdom*
⁹⁵*Indian Institute of Technology, Gandhinagar Ahmedabad Gujarat 382424, India*
⁹⁶*Institute for Plasma Research, Bhat, Gandhinagar 382428, India*
⁹⁷*University of Szeged, Dóm tér 9, Szeged 6720, Hungary*
⁹⁸*Embry-Riddle Aeronautical University, Prescott, AZ 86301, USA*
⁹⁹*University of Michigan, Ann Arbor, MI 48109, USA*
¹⁰⁰*Tata Institute of Fundamental Research, Mumbai 400005, India*
¹⁰¹*American University, Washington, D.C. 20016, USA*
¹⁰²*Rochester Institute of Technology, Rochester, NY 14623, USA*
¹⁰³*University of Massachusetts-Amherst, Amherst, MA 01003, USA*
¹⁰⁴*University of Adelaide, Adelaide, South Australia 5005, Australia*
¹⁰⁵*West Virginia University, Morgantown, WV 26506, USA*
¹⁰⁶*University of Białystok, 15-424 Białystok, Poland*
¹⁰⁷*SUPA, University of Strathclyde, Glasgow G1 1XQ, United Kingdom*
¹⁰⁸*IISER-TVM, CET Campus, Trivandrum Kerala 695016, India*
¹⁰⁹*Institute of Applied Physics, Nizhny Novgorod, 603950, Russia*
¹¹⁰*Pusan National University, Busan 609-735, Korea*
¹¹¹*Hanyang University, Seoul 133-791, Korea*
¹¹²*NCBJ, 05-400 Świerk-Otwock, Poland*
¹¹³*IM-PAN, 00-956 Warsaw, Poland*
¹¹⁴*Monash University, Victoria 3800, Australia*
¹¹⁵*Seoul National University, Seoul 151-742, Korea*
¹¹⁶*University of Alabama in Huntsville, Huntsville, AL 35899, USA*
¹¹⁷*ESPCI, CNRS, F-75005 Paris, France*
¹¹⁸*Università di Camerino, Dipartimento di Fisica, I-62032 Camerino, Italy*
¹¹⁹*Southern University and A&M College, Baton Rouge, LA 70813, USA*
¹²⁰*College of William and Mary, Williamsburg, VA 23187, USA*
¹²¹*Instituto de Física Teórica, University Estadual Paulista/ICTP South American Institute for Fundamental Research, São Paulo SP 01140-070, Brazil*
¹²²*University of Cambridge, Cambridge CB2 1TN, United Kingdom*
¹²³*IISER-Kolkata, Mohanpur, West Bengal 741252, India*
¹²⁴*Rutherford Appleton Laboratory, HSIC, Chilton, Didcot, Oxon OX11 0QX, United Kingdom*
¹²⁵*Whitman College, 345 Boyer Avenue, Walla Walla, WA 99362 USA*
¹²⁶*National Institute for Mathematical Sciences, Daejeon 305-390, Korea*
¹²⁷*Hobart and William Smith Colleges, Geneva, NY 14456, USA*
¹²⁸*Janusz Gil Institute of Astronomy, University of Zielona Góra, 65-265 Zielona Góra, Poland*
¹²⁹*Andrews University, Berrien Springs, MI 49104, USA*
¹³⁰*Caltech JPL, Pasadena, CA 91109, USA*
¹³¹*Università di Siena, I-53100 Siena, Italy*
¹³²*Trinity University, San Antonio, TX 78212, USA*
¹³³*University of Washington, Seattle, WA 98195, USA*
¹³⁴*Kenyon College, Gambier, OH 43022, USA*
¹³⁵*Abilene Christian University, Abilene, TX 79699, USA*

(Dated: December 3, 2024)

The LIGO detection of GW150914 provides an unprecedented opportunity to study the two-body motion of a compact-object binary in the large velocity, highly nonlinear regime, and to witness the final merger of the binary and the excitation of uniquely relativistic modes of the gravitational field. We carry out several investigations to determine whether GW150914 is consistent with a binary black-hole merger in general relativity. We find that the final remnant's mass and spin, as determined from the low-frequency (inspiral) and high-frequency (post-inspiral) phases of the signal, are mutually consistent with the binary black-hole solution in general relativity. Furthermore, the data following the peak of GW150914 are consistent with the least-damped quasi-normal mode inferred from the mass and spin of the remnant black hole. By using waveform models that allow for parameterized general-relativity violations during the inspiral and merger phases, we perform quantitative tests on the gravitational-wave phase in the dynamical regime and we determine the first empirical bounds on several high-order post-Newtonian coefficients. We constrain the graviton Compton wavelength, assuming that gravitons are dispersed in vacuum in the same way as particles with mass, obtaining a 90%-confidence lower bound of 10^{13} km. In conclusion, within our statistical uncertainties, we find no evidence for violations of general relativity in the genuinely strong-field regime of gravity.

Introduction. On September 14, 2015, at 09:50:45 Universal Time, the LIGO detectors at Hanford, Washington and

Livingston, Louisiana, detected a gravitational-wave (GW)

signal, henceforth GW150914, with an observed signal-to-noise ratio (SNR) ~ 24 . The probability that GW150914 was due to a random noise fluctuation was later established to be $< 2 \times 10^{-7}$ [1, 2]. GW150914 exhibited the expected signature of an inspiral, merger, and ringdown signal from a coalescing binary system [1]. Assuming that general relativity (GR) is the correct description for GW150914, detailed follow-up analyses determined the (detector-frame) component masses of the binary system to be $39_{-4}^{+6} M_{\odot}$ and $32_{-5}^{+4} M_{\odot}$ at 90% credible intervals [3], corroborating the hypothesis that GW150914 was emitted by a binary black hole.

In Newtonian gravity, binary systems move along circular or elliptical orbits with constant orbital period [4, 5]. In GR, binary systems emit GWs [6, 7]; as a consequence, the binary's orbital period decreases over time as energy and angular momentum are radiated away. Electromagnetic observations of binary pulsars over the four decades since their discovery [8, 9] have made it possible to measure GW-induced orbital-period variations $\dot{P}_{\text{orb}} \sim -10^{-14} \text{--} 10^{-12}$, confirming the GW luminosity predicted at leading order in post-Newtonian (PN) theory [10] (i.e., Einstein's quadrupole formula) with exquisite precision [11, 12]. Nevertheless, even in the most relativistic binary pulsar known today, J0737-3039 [11], the orbital period changes at an effectively constant rate. The orbital velocity v relative to the speed of light c is $v/c \sim 2 \times 10^{-3}$, and the two neutron stars in the system will coalesce in ~ 85 Myr.

By contrast, GW150914 was emitted by a rapidly evolving, dynamical binary that swept through the detectors' bandwidth and merged in a fraction of a second, with \dot{P}_{orb} ranging from ~ -0.1 at $f_{\text{GW}} \sim 30$ Hz to ~ -1 at $f_{\text{GW}} \sim 132$ Hz (just before merger, where v/c reached ~ 0.5). Thus, through GW150914 we observe the two-body motion in the large-velocity, highly dynamical, strong-field regime of gravity, leading to the formation of a new merged object, and generating GWs. While Solar-System experiments, binary-pulsar observations, and cosmological measurements are all in excellent agreement with GR (see Refs. [12–14] and references therein), they test it in low-velocity, quasi-static, weak-field, or linear regimes.¹ Thus, GW150914 opens up the distinct opportunity of probing unexplored sectors of GR.

Here we perform several studies of GW150914, aimed at detecting deviations from the predictions of GR. Within the limits set by LIGO's sensitivity and by the nature of GW150914, we find no statistically significant evidence against the hypothesis that GW150914 was emitted by two black holes spiraling towards each other and merging to form a single, rotating black hole [17, 18], and that the dynamics of the process as a whole was in accordance with the vacuum Einstein field equations.

We begin by constraining the level of coherent (i.e., GW-like) residual strain left after removing the most-probable GR waveform from the GW150914 data, and use this estimated level to bound GR violations which are not degenerate with changes in the parameters of the binary. We then verify that the mass and spin parameters of the final black hole, as predicted from the binary's inspiral signal, are consistent with the final parameters inferred from the post-inspiral (merger and ringdown) signal. We find that the data following the peak of GW150914 are consistent with the least-damped quasi-normal mode (QNM) inferred from the final black-hole's characteristics. Next, we perform targeted measurements of the PN and phenomenological coefficients that parameterize theoretical waveform models, and find no tension with the values predicted in GR and numerical-relativity (NR) simulations. Furthermore, we search for evidence of dispersion in the propagation of GW150914 toward the Earth, as it would appear in a theory in which the graviton is assigned a finite Compton wavelength (i.e., a nonzero mass). Finally, we show that, due to the LIGO network configuration, we cannot exclude the presence of non-GR polarization states in GW150914.

As we shall see, the constraints on the strong-field dynamics of gravity obtained from GW150914 are not yet very tight; for instance, some of the bounds on relative deviations in PN parameters are $\mathcal{O}(1)$. On the other hand, it is to be noted that the LIGO detectors are still a factor of a few away from their final design sensitivities [19], and even louder sources than GW150914 may be seen in the near future; moreover, as more detections are made, we will be able to combine information from all observed sources to obtain progressively sharper bounds on PN and other coefficients.

In the rest of this paper, when reporting physical quantities that are redshifted in the transformation between the source and detector frames, we refer to the detector frame unless we specify otherwise.

Waveform models, systematics, and statistical effects. Tests of GR from GW observations build on the knowledge of the gravitational waveform in GR, and on the statistical properties of instrumental noise. Any uncontrolled systematic effect from waveform modeling and/or the detectors could in principle affect the outcome of our tests. Thus, we begin by checking that these uncertainties are either below our measurement precision or accounted for.

The analytical inspiral-merger-ringdown (IMR) waveform models used in this paper were developed within two frameworks: i) the effective-one-body (EOB) formalism [20–24], which combines PN results [10] with NR [25–27] and perturbation theory [28–30], and ii) a phenomenological approach [31–34] based on extending frequency-domain PN expressions and hybridizing PN/EOB with NR waveforms. In particular, here we adopt the double-spin, nonprecessing waveform model developed in Ref. [35] using NR waveforms from Ref. [36], enhanced with reduced-order modeling [37] to speed up waveform generation [38, 39] (henceforth, EOBNR), and the single-effective-spin, precessing waveform model of

¹ While the orbits of binary pulsars are weakly relativistic, pulsars themselves are strongly self-gravitating bodies, so they do offer opportunities to test strong-field gravity [15, 16].

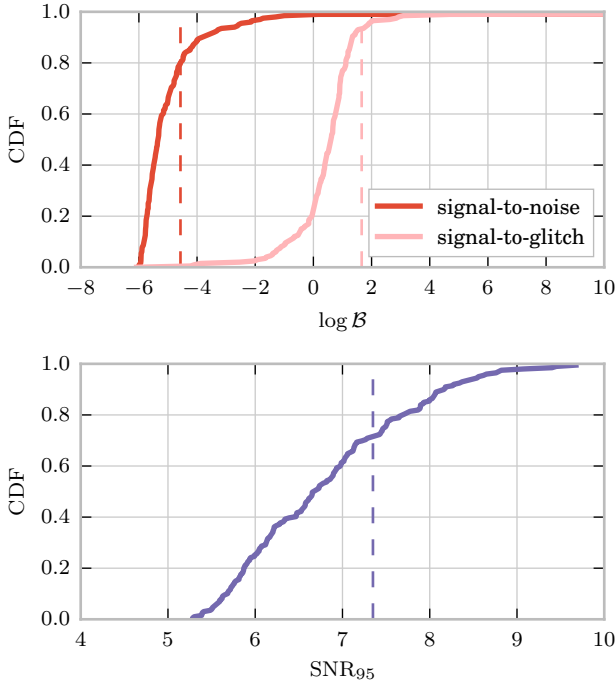


FIG. 1. Upper panel: cumulative distribution function (CDF) of log Bayes factor – the logarithm of the ratio of Bayesian evidences between two competing models – for the signal-versus-noise and signal-versus-glitch BAYESWAVE models, computed for 100 4-s stretches of data around GW150914. Lower Panel: cumulative distribution function (CDF) of the 95% credible upper bound on network coherent-burst SNR, denoted SNR_{95} , again computed for 100 instrument-noise segments. In both panels, we indicate with dashed lines the log Bayes factors and upper bound on coherent-burst SNR corresponding to the residuals obtained after subtracting the most probable waveform from GW150914.

Refs. [40–42] (henceforth, IMRPHENOM).² Both models are calibrated against waveforms from direct numerical integration of the Einstein equations.

As shown in Refs. [3, 35, 41, 43, 44], in the region of parameter space relevant for GW150914, the error due to differences between the two analytical waveform models (and between the analytical and numerical-relativity waveforms) is smaller than the typical statistical uncertainty due to the finite SNR of GW150914. To assess potential modeling systematics, we collected existing NR waveforms and generated new, targeted simulations. The simulations were generated with multiple independent codes [45–50], and sample the posterior region for the masses and spins inferred for GW150914 [3]. Since the posteriors for the magnitudes and orientations of the component spins are not very constraining, the choices for these parameters covered wide ranges. To validate the stud-

ies below, we added the publicly available and new NR waveforms as mock signals to the data in the neighbourhood of GW150914 [36, 50, 51]. A further possible cause for systematics are uncertainties in the calibration of the gravitational-strain observable in the LIGO detectors. These uncertainties are modeled and included in the results presented here according to the treatment detailed in Ref. [3].

Residuals after subtracting the most-probable waveform model. The burst analysis [52], which looks for unmodeled transients and hence does not rely on theoretical signal templates, can be used to test the consistency of GW150914 with waveform models derived from GR. Using the LALINFERENCE [53] Bayesian-inference software library, we identify the most probable (i.e., *maximum a posteriori*, henceforth MAP) binary black-hole waveform [3], compute its effect in the Livingston and Hanford detectors, and then subtract it from the data. If the data are consistent with the theoretical signal, no detectable power should remain after subtraction other than what is consistent with instrumental noise. We analyze the residual with the BAYESWAVE [54] algorithm developed to characterize generic GW transients. BAYESWAVE uses the evidence ratio (Bayes factor) to rank competing hypotheses given the observed data. We compare predictions from models in which: (i) the data contain only Gaussian noise; (ii) the data contain Gaussian noise and uncorrelated noise transients, or glitches, and (iii) the data contain Gaussian noise and an elliptically polarized GW signal. We compute the signal-to-noise Bayes factor, which is a measure of significance for the excess power in the data, and the signal-to-glitch Bayes factor, which measures the coherence of the excess power between the two detectors.

Our analysis reveals that the GW150914 residual favors the instrumental noise hypothesis over the presence of a coherent signal as well as the presence of glitches in either detectors; see the dashed lines in the top panel of Fig. 1. The positive Bayes factor for the signal-to-glitch hypotheses indicates that the data prefer the presence of a coherent signal over glitches; nevertheless, the signal remains below common significance thresholds, as indicated by the limit on the residual SNR_{res} given in the lower panel of Fig. 1 and further explained below. This is an indication of the stability of the LIGO detectors at the time of GW150914. We also apply the same analysis to 100 4-second long segments of data drawn within a few minutes of GW150914, and produce the cumulative distribution functions of Bayes factors shown in the upper panel of Fig. 1. We find that, according to the burst analysis, the GW150914 residual is not statistically distinguishable from the instrumental noise recorded in the vicinity of the detection, suggesting that all of the measured power is well represented by the GR prediction for the signal from a binary black-hole merger. The results of this analysis are very similar regardless of the MAP waveform used (i.e., EOBNR or IMRPHENOM).

We compute the 95% upper bound on the coherent network SNR_{res} . This upper bound is $\text{SNR}_{\text{res}} \leq 7.3$ at 95% confidence, independently of the MAP waveform used (i.e., EOBNR or IMRPHENOM). We note that this coherent-burst SNR has a dif-

² The specific names of the two waveform models that we use in the LIGO ALGORITHM LIBRARY are SEOBNRv2_ROM_DOUBLESPIN and IMRPHENOMv2.

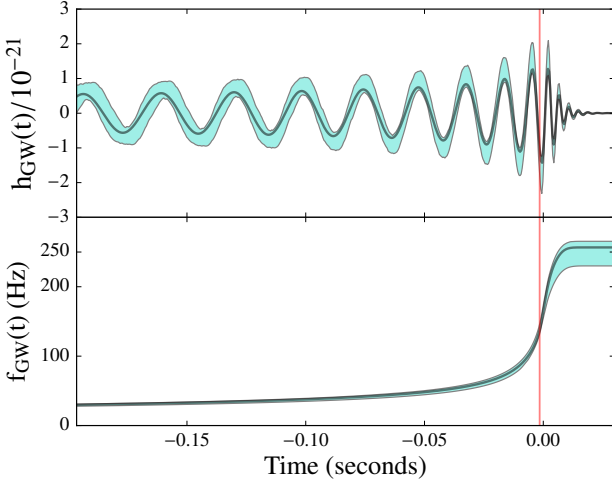


FIG. 2. MAP estimate and 90% credible regions for the waveform (upper panel) and GW frequency (lower panel) of GW150914 as estimated by the LALINFERECE analysis [3]. The solid lines in each panel indicate the most probable waveform from GW150914 [3] and its GW frequency. We mark with a vertical line the instantaneous frequency $f_{\text{GW}}^{\text{endinsp}} = 132$ Hz, which is used in the IMR consistency test to delineate the boundary between the frequency-domain inspiral and post-inspiral parts (see Fig. 3 below for a representation of the most probable waveform’s amplitude in frequency domain).

ferent meaning compared to the (modeled) matched-filtering binary-coalescence SNR of 24 cited for GW150914. Indeed, the upper-limit SNR_{res} inferred for GW150914 lies in the typical range for the data segments around GW150914 (see the bottom panel of Fig. 1), so it can be attributed to instrument noise alone.

If we assume that SNR_{res} is entirely due to the mismatch between the MAP waveform and the underlying true signal, and that the putative violation of GR cannot be reabsorbed in the waveform model by biasing the estimates of the physical parameters [55, 56], we can constrain the minimum *fitting factor* (FF) [57] between the MAP model and GW150914. An imperfect fit to the data leaves $\text{SNR}_{\text{res}}^2 = (1 - \text{FF}^2) \text{FF}^{-2} \text{SNR}_{\text{det}}^2$ [58, 59] where $\text{SNR}_{\text{det}} = 25.3^{+0.1}_{-0.2}$ is the network SNR inferred by LALINFERECE [3]. $\text{SNR}_{\text{res}} \leq 7.3$ then implies $\text{FF} \geq 0.96$. Considering that, for parameters similar to those inferred for GW150914, our waveform models have much higher FFs against numerical GR waveforms, we conclude that the noise-weighted correlation between the observed strain signal and the true GR waveform is $\geq 96\%$. This statement can be read as implying that the GR prediction for GW150914 is verified to better than 4%, in a precise sense related to noise-weighted signal correlation; and conversely, that effects due to GR-violations in GW150914 are limited to less than 4% (for effects that cannot be reabsorbed in a redefinition of physical parameters).

Inspiral–merger–ringdown consistency test. We now perform a test to show that the entire GW150914 waveform does not deviate from the predictions of a binary black-hole coa-

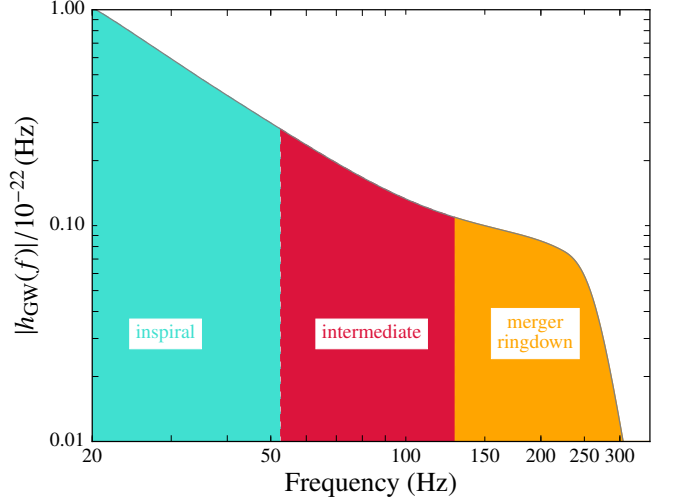


FIG. 3. Frequency regions of the parameterized waveform model as defined in the text and in Ref. [41]. The plot shows the absolute value of the frequency-domain amplitude of the most-probable waveform from GW150914 [3]. The inspiral region (cyan) from 20 Hz to ~ 55 Hz corresponds to the early and late inspiral regimes. The intermediate region (red) goes from ~ 55 Hz to ~ 130 Hz. Finally, the merger–ringdown region (orange) goes from ~ 130 Hz to the end of the waveform.

lescence in GR. One way to do that is to compare the estimates of the mass and spin of the remnant obtained from the low-frequency and high-frequency parts of the waveform, using the relations between the binary’s components and final masses and spins provided by NR [60].

For the purpose of this test, we choose $f_{\text{GW}}^{\text{endinsp}} = 132$ Hz as the frequency at which the late inspiral phase ends. In Fig. 2 we plot the EOBNR MAP waveform [3] and its 90% credible intervals, as well as the corresponding instantaneous frequency; the vertical line marks $f_{\text{GW}}^{\text{endinsp}}$. Fig. 3 shows the frequency-domain MAP waveform amplitude; note that 132 Hz lies just before what is generally denoted as the merger–ringdown phase in the frequency domain.

To perform the test, we first truncate the frequency-domain representation of the waveforms to lie between 20 Hz to $f_{\text{GW}}^{\text{endinsp}}$, and we estimate the posterior distributions of the binary’s component masses and spins using this “inspiral” (low-frequency) part of the observed signal, using the nested-sampling algorithm in the LALINFERECE software library [53]. We then use formulae obtained from NR simulations to compute posterior distributions of the remnant’s mass and spin. Next, we obtain the complementary “post-inspiral” (high-frequency) signal, which is dominated by the contribution from the merger and ringdown stages, by restricting the frequency-domain representation of the waveforms to extend between $f_{\text{GW}}^{\text{endinsp}}$ and 1024 Hz. Again, we derive the posterior distributions of the component masses and spins, and (by way of NR-derived formulae) of the mass and spin of the final compact object. We note that the MAP waveform has an expected $\text{SNR}_{\text{det}} \sim 19.5$ if we truncate its frequency-domain

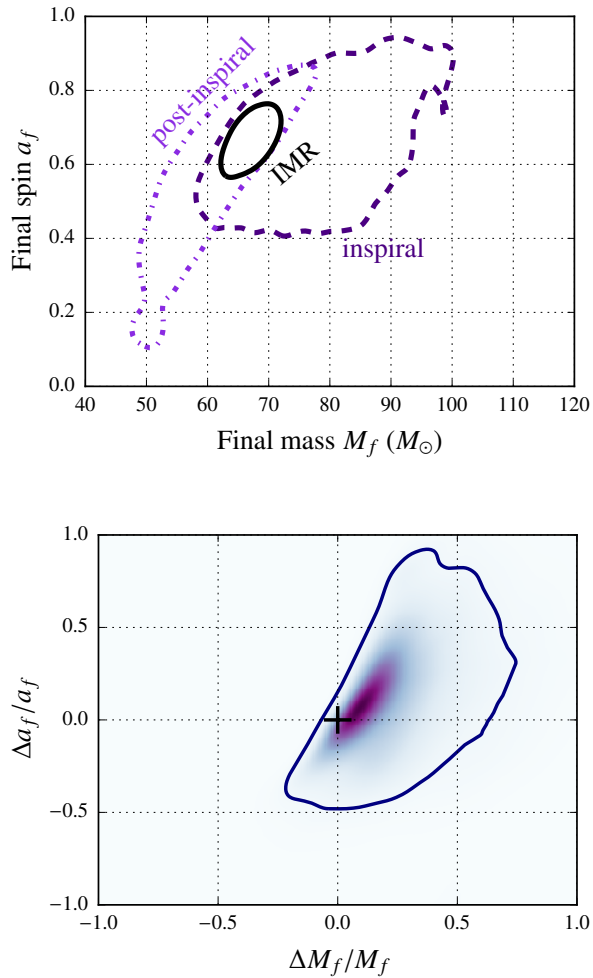


FIG. 4. *Top panel*: 90% credible regions in the joint posterior distributions for the mass M_f and dimensionless spin a_f of the final compact object as determined from the inspiral (dark violet, dashed) and post-inspiral (violet, dot-dashed) signals, and from a full inspiral-merger-ringdown analysis (black). *Bottom panel*: Posterior distributions for the parameters $\Delta M_f / M_f$ and $\Delta a_f / a_f$ that describe the fractional difference in the estimates of the final mass and spin from inspiral and post-inspiral signals. The contour shows the 90% confidence region. The plus symbol indicates the expected GR value $(0, 0)$.

representation to have support between 20 and 132 Hz, and ~ 16 if we truncate it to have support between 132 and 1,024 Hz. Finally, we compare these two estimates of the final M_f and dimensionless spin a_f , and compare them also against the estimate performed using full inspiral-merger-ringdown waveforms. In all cases, we average the posteriors obtained with the EOBNR and IMRPhenom waveform models, following the procedure outlined in Ref. [3]. Technical details about the implementation of this test can be found in Ref. [61].

This test is similar in spirit to the χ^2 GW search statistic [2, 62], which divides the model waveform into frequency bands and checks that the SNR accumulates as expected

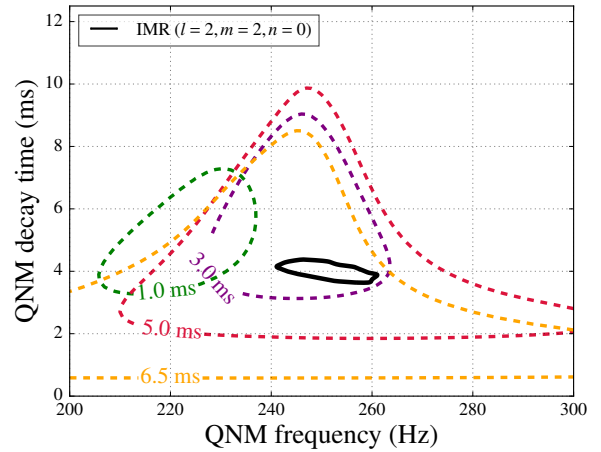


FIG. 5. 90% credible regions in the joint posterior distributions for the damped-sinusoid parameters f_0 and τ (see main text), assuming start times $t_0 = t_M + 1, 3, 5, 6.5$ ms, where t_M is the merger time of the MAP waveform for GW150914. The black solid line shows the 90% credible region for the frequency and decay time of the $\ell = 2, m = 2, n = 0$ (i.e., the least damped) QNM, as derived from the posterior distributions of the remnant mass and spin parameters.

across those bands. Large matched-filter SNR values which are accompanied by large χ^2 statistic are very likely due either to noise glitches, or to a mismatch between the signal and the model matched-filter waveform. Conversely, reduced- χ^2 values near unity indicate that the data are consistent with waveform plus the expected detector noise. Thus, large χ^2 values are a warning that some parts of the waveform are fit much worse than others, and thus the candidates may be due to instrument glitches that are very loud, but do not resemble binary-inspiral signals. However, χ^2 tests are performed by comparing the data with a single theoretical waveform, while in this case we allow the inspiral and post-inspiral partial waveforms to select different physical parameters. Thus, this test should be sensitive to subtler deviations from the predictions of GR.

In Fig. 4 we summarize our findings. The top panel shows the posterior distributions of M_f and a_f estimated from the inspiral and post-inspiral signals, and from the entire inspiral-merger-ringdown waveform. The plot confirms the expected behavior: the inspiral and post-inspiral 90% confidence regions (defined by the isoprobability contours that enclose 90% of the posterior) have a significant region of overlap. As a sanity check (which strictly speaking is not part of the test of GR that is being performed) we also produced the 90% confidence region computed with the full inspiral-merger-ringdown waveform; it lies comfortably within this overlap. We have verified that these conclusions are not affected by the specific formula [40, 60, 63] used to predict M_f and a_f , nor by the choice of $f_{GW}^{\text{end,insp}}$ within ± 50 Hz.

To assess the significance of our findings more quantitatively, we define parameters $\Delta M_f / M_f$ and $\Delta a_f / a_f$ that describe the fractional difference between the two estimates of

the final mass and spin, and calculate their joint posterior distribution, using for (M_f, a_f) the posterior distribution obtained from the full IMR waveform; see [61] for explicit expressions. The result is shown in the bottom panel of Fig. 4; the solid line marks the isoprobability contour that contains 90% of the posterior. The plus symbol indicates the null $(0, 0)$ result expected in GR, which lies on the isoprobability contour that encloses 28% of the posterior.

We have checked that if we perform this analysis on NR signals added to LIGO instrumental noise, the null $(0, 0)$ result expected in GR lies within the iso-probability contour that encloses 68% of the posterior roughly 68% of the time, as expected from random noise fluctuations. By contrast, our test can rule out the null hypothesis (with high statistical significance) when analyzing a simulated signal that reflects a significant GR violation in the frequency dependence of the energy and angular momentum loss [61], even when we choose violations which would be too small to be noticeable in double-pulsar observations [12]; for an explicit example we refer to Fig. 1 of Ref. [61]. This includes signals with χ^2 value close to unity, so that they would not have been missed by the modeled-signal searches. Thus, our inspiral–merger–ringdown test shows no evidence of discrepancies with the predictions of GR.

The component masses and spins estimated in Ref. [3], together with NR-derived relations, imply $M_f = 68^{+4}_{-4} M_\odot$ ($62^{+4}_{-4} M_\odot$ in the source frame) and $a_f = 0.67^{+0.05}_{-0.07}$ at 90% confidence. From the posterior distributions of the mass and spin of the final black hole, we can predict the frequency and decay time of the least-damped QNM (i.e., the $\ell = 2, m = 2, n = 0$ overtone) [64]. We find $f_{220}^{\text{QNM}} = 251^{+8}_{-8}$ Hz and $\tau_{220}^{\text{QNM}} = 4.0^{+0.3}_{-0.3}$ ms at 90% confidence.

Testing for the least-damped QNM in the data. We perform a test to check the consistency of the data with the predicted least-damped QNM of the remnant black hole. For this purpose we compute the Bayes factor between a damped-sinusoid waveform model and Gaussian noise, and estimate the corresponding parameter posteriors. The signal model used is $h(t \geq t_0) = A e^{-(t-t_0)/\tau} \cos[2\pi f_0(t-t_0) + \phi_0]$, $h(t < t_0) = 0$, with fixed starting time t_0 , and uniform priors over the unknown frequency $f_0 \in [200, 300]$ Hz and damping time $\tau \in [0.5, 20]$ ms. The prior on amplitude A and phase ϕ_0 is chosen as a two-dimensional Gaussian isotropic prior in $\{A_s \equiv -A \sin \phi_0, A_c \equiv A \cos \phi_0\}$ with a characteristic scale H , which is in turn marginalized over the range $H \in [2, 10] \times 10^{-22}$ with a prior $\propto 1/H$. This is a practical choice that encodes relative ignorance about the detectable damped-sinusoid amplitude in this range. We use 8 s of data (centered on GW150914) from both detectors, band-passed to [20, 1900] Hz. The data are analyzed coherently, assuming the signal arrived 7 ms earlier at Livingston compared to Hanford, and the amplitude received in the two detectors has approximately equal magnitude and opposite sign (as seen in e.g. Fig. 1 of [1]).

We compute the Bayes factor and posterior estimates of $\{f_0, \tau\}$ as a function of the unknown QNM start-time t_0 , which

we parameterize as an offset from a fiducial GPS merger time³ $t_M = 1,126,259,462.423$ s (at the LIGO Hanford site). Figure 5 shows the 90% credible contours in the $\{f_0, \tau\}$ plane as a function of the merger-to-start time offset $t_0 - t_M$, as well as the corresponding contour for the least-damped QNM as predicted in GR for the remnant mass and spin parameters estimated for GW150914.

The 90% posterior contour starts to overlap with GR prediction from the IMR waveform for $t_0 = t_M + 3$ ms, or $\sim 10 M$ after merger. The corresponding log Bayes factor at this point is $\log_{10} B \sim 14$ and the MAP waveform SNR is ~ 8.5 . For $t_0 = t_M + 5$ ms the MAP parameters fall within the contour predicted in GR for the least-damped QNM, with $\log_{10} B \sim 6.5$ and SNR ~ 6.3 . At $t_0 = t_M + 6.5$ ms, or about $20 M$ after merger, the Bayes factor is $\log_{10} B \sim 3.5$ with SNR ~ 4.8 . The signal becomes undetectable shortly thereafter, for $t_0 \gtrsim t_M + 9$ ms, where $B \lesssim 1$.

Measuring the frequency and decay time of *one* damped sinusoid in the data does not by itself allow us to conclude that we have observed the least-damped QNM of the final black hole, since the measured quality factor could be biased by the presence of the other QNMs in the ringdown signal (see, e.g., Ref. [64, 65] and references therein). However, based on the numerical simulations discussed in Refs. [66–68], one should expect the GW frequency to level off at $10 - 20 M$ after the merger, which is where the description of ringdown in terms of QNMs becomes valid. For a mass $M \sim 68 M_\odot$, the corresponding range is $\sim 3 - 7$ ms after merger. Since this is where we observe the 90% posterior contours of the damped-sinusoid waveform model and the 90% confidence region estimated from the IMR waveform to be consistent with each other, we may conclude that the data are compatible with the presence of the least-damped QNM as predicted by GR.

In the future, we will extend the analysis to two damped sinusoids, and explore the possibility of independently extracting the final black hole’s mass and spin. A test of the general relativistic no-hair theorem [69, 70] requires the identification of at least two QNM frequencies in the ringdown waveform [65, 71, 72]. Such a test would benefit from the observation of a system with a total mass similar to the one of GW150914, but with a larger asymmetry between component masses, which would increase the amplitudes of the sub-dominant modes; a stronger misalignment of the orbital angular momentum with the line of sight would further improve their visibility [71]. Finally, the determination of the remnant mass and spin independently of binary component parameters will allow us to test the second law of black-hole dynamics [73, 74].

Constraining parameterized deviations from general-relativistic inspiral–merger–ringdown waveforms. Because

³ The merger time is obtained by taking the EOBNR MAP waveform and lining this waveform up with the data such that the largest SNR is obtained. The merger time is then defined as the point at which the quadrature sum of the h_+ and h_\times polarizations is maximum.

GW150914 was emitted by a binary black hole in its final phase of rapid orbital evolution, its gravitational phasing (or phase evolution) encodes nonlinear conservative and dissipative effects that are not observable in binary pulsars, whose orbital period changes at an approximately constant rate.⁴ Those effects include tails of radiation due to backscattering of GWs by the curved background around the coalescing black holes [75], nonlinear tails (i.e., tails of tails) [76], couplings between black-hole spins and the binary’s orbital angular momentum, interactions between the spins of the two bodies [77–79], and excitations of QNMs [28–30] as the remnant black hole settles in the stationary configuration.

Whether all these subtle effects can actually be identified in GW150914 and tested against GR predictions depends of course on their strength with respect to instrument noise and on whether the available waveform models are parameterized in terms of those physical effects. GW150914 is moderately loud, with $\text{SNR} \sim 24$, certainly much smaller than what can be achieved in binary-pulsar observations. Our ability to analyze the fine structure of the GW150914 waveform is correspondingly limited. Our approach is to adopt a parameterized analytical family of inspiral–merger–ringdown waveforms, then treat the waveform coefficients as free variables that can be estimated (either individually or in groups) from the GW150914 data [80–86]. We can then verify that the posterior probability distributions for the coefficients include their GR values.

The simplest and fastest parameterized waveform model that is currently available [41] can be used to bound physical effects only for the coefficients that enter the early inspiral phase, because for the late inspiral, merger, and ringdown phases it uses phenomenological coefficients fitted to NR waveforms. Louder GW events, to be collected as detector sensitivity improves, and more sophisticated parameterized waveform models, will allow us to do much more stringent and physical tests targeted at specific relativistic effects. We work within a subset of the TIGER framework [86, 87] and perform a null-hypothesis test by comparing GW150914 with a *generalized*, analytical inspiral–merger–ringdown waveform model (henceforth, gIMR) that includes parameterized deformations with respect to GR. In this framework, deviations from GR are modeled as *fractional changes* $\{\delta\hat{p}_i\}$ in any of the parameters $\{p_i\}$ that parameterize the GW phase expression in the baseline waveform model. Similarly to Refs. [86, 87], we only consider deviations from GR in the GW phase, while we leave the GW amplitude unperturbed. Indeed, at the SNR of GW150914 (i.e., $\text{SNR} \sim 24$), we expect to have much higher sensitivity to the GW phase rather than to its amplitude. Also, amplitude deviations could be reabsorbed in the calibration error model used to analyze GW150914 [3].

⁴ Current binary-pulsar observations do constrain conservative dynamics at 1PN order and they partially constrain spin–orbit effects at 1.5PN order through geodetic spin precession [12].

We construct gIMR starting from the frequency-domain IMRPhenom waveform model. The dynamical stages that characterize the coalescence process can be represented in the frequency-domain by plotting the absolute value of the waveform’s amplitude. We review those stages in Fig. 3 to guide the reader towards the interpretation of the results that are summarized in Table I and Figs. 6 and 7. We refer to the *early-inspiral stage* as the PN part of the GW phase. This stage of the phase evolution is known analytically up to $(v/c)^7$ and it is parameterized in terms of the PN coefficients φ_j , $j = 0, \dots, 7$ and the *logarithmic* terms φ_{jl} , $j = 5, 6$. The *late-inspiral stage*, parameterized in terms of σ_j , $j = 1, \dots, 4$, is defined as the phenomenological extension of the PN series to $(v/c)^{11}$. The *early* and *late inspiral* stages are denoted simply as *inspiral* both in Ref. [41] and in Fig. 3. The *intermediate stage* that models the transition between the inspiral and the merger–ringdown phase is parameterized in terms of the phenomenological coefficients β_j , $j = 1, 2, 3$. Finally, the *merger–ringdown* phase is parameterized in terms of the phenomenological coefficients α_j , $j = 1, 2, 3$. The β_j and α_j aim to capture the frequency dependences of the phase of the corresponding regimes; see the column “*f*–dependence” in Table I. Due to the procedure through which the model is constructed, which involves fitting a waveform phasing ansatz to a calibration set of EOB waveforms joined to NR waveforms [41], there is an intrinsic uncertainty in the values of the phenomenological parameters of the IMRPhenom model. For the intermediate and merger–ringdown regime, we verified that these intrinsic uncertainties are much smaller than the corresponding statistical uncertainties for GW150914, and thus do not affect our conclusions. In the late-inspiral case, the uncertainties associated with the calibration of the σ_j parameters are large, and almost comparable with the statistical measurement uncertainties. For this reason, we do not report results for the σ_j parameters.

As said, we construct the gIMR model by introducing (fractional) deformations $\delta\hat{p}_i$ for each of the IMRPhenom phase parameters p_i , which dominate the evolution of the phase at the different stages in the coalescence explained above. At each point in parameter space, the coefficients p_i are evaluated for the local physical parameters (masses, spins) and multiplied by factors $(1 + \delta\hat{p}_i)$. When using such waveforms as templates, the parameters that are allowed to vary freely are then the ones that are also present in the GR waveforms (masses, spins, sky position, orientation, distance, and a reference time and phase), together with one or more of the $\delta\hat{p}_i$; the p_i themselves are calculated using their GR expressions in terms of masses and spins. In this parameterization, GR is uniquely defined as the locus in the parameter space where all of the testing parameters $\delta\hat{p}_i$ are zero. In summary, our battery of testing parameters consists of: (i) early-inspiral stage: $\{\delta\hat{\varphi}_0, \delta\hat{\varphi}_1, \delta\hat{\varphi}_2, \delta\hat{\varphi}_3, \delta\hat{\varphi}_4, \delta\hat{\varphi}_{5l}, \delta\hat{\varphi}_6, \delta\hat{\varphi}_{6l}, \delta\hat{\varphi}_7\}$ ⁵, (ii) intermediate regime: $\{\delta\hat{\beta}_2, \delta\hat{\beta}_3\}$, and (iii) merger–ringdown regime:

⁵ Unlike Ref. [41], we explicitly include the logarithmic terms $\delta\hat{\varphi}_{5l}$ and $\delta\hat{\varphi}_{6l}$.

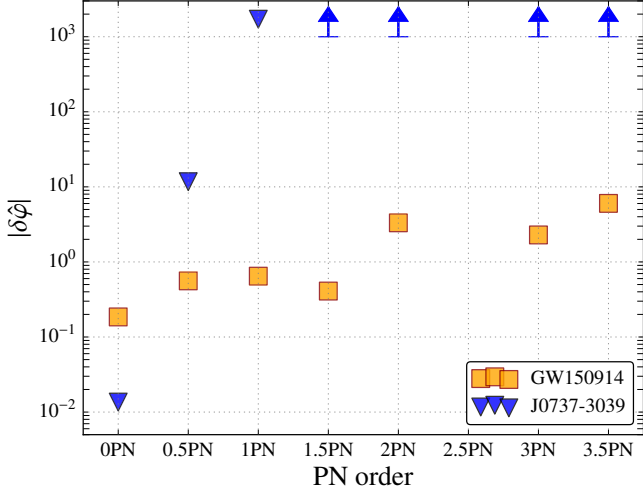


FIG. 6. 90% upper bounds on the fractional variations of the known PN coefficients with respect to their GR values. The orange squares are the 90% upper bounds obtained from the single-parameter analysis of GW150914. As a comparison, the blue triangles show the 90% upper bounds extrapolated exclusively from the measured orbital-period derivative \dot{P}_{orb} of the double pulsar J0737-3039 [12, 88], here too allowing for possible GR violations at different powers of frequency, one at a time. The GW phase deduced from an almost constant \dot{P}_{orb} cannot provide significant information as the PN order is increased, so we show the bounds for the latter only up to 1PN order. We do not report on the deviation of the 2.5PN coefficient, which is unmeasurable because it is degenerate with the reference phase. We also do not report on the deviations of the logarithmic terms in the PN series at 2.5PN and 3PN order, which can be found in Table I and in Fig. 7.

$\{\delta\hat{\alpha}_2, \delta\hat{\alpha}_3, \delta\hat{\alpha}_4\}$. We do not consider parameters that are degenerate with either the reference time or the reference phase. For our analysis, we explore two scenarios: *single-parameter* analysis, in which only one of the testing parameters is allowed to vary freely (in addition to masses, spins, ...) while the remaining ones are fixed to their GR value, that is zero, and *multiple-parameter* analysis in which all the parameters in one of the three sets enumerated above are allowed to vary simultaneously.

The rationale behind our choices of single- and multiple-parameter analyses comes from the following considerations. In most known alternative theories of gravity [13, 14, 89], the corrections to GR extend to all PN orders even if in most cases they have been computed only at leading PN order. Considering that GW150914 is an inspiral–merger–ringdown signal sweeping through the detector between 20 Hz and 300 Hz, we expect to see signal deviations from GR at all PN orders. The single-parameter analysis corresponds to minimally extended models that can capture deviations from GR that occur predominantly, but not only, at a specific PN order. Nevertheless,

We also include the 0.5PN parameter $\delta\hat{\varphi}_1$; since φ_1 is zero in GR, we define $\delta\hat{\varphi}_1$ to be an absolute shift rather than a fractional deformation.

less, should a deviation be measurably present at multiple PN orders, we expect the single-parameter analyses to also capture these. In the multiple-parameter analysis, the correlations among the parameters are very significant. In other words, a shift in one of the testing parameters can always be compensated by a change of the opposite sign in another parameter, and still return the same overall GW phase. Thus, it is not surprising that the multiple-parameter case provides a much more conservative statement on the agreement between GW150914 and GR. We defer to future studies the identification of optimally determined directions in the $\delta\hat{\beta}_i$ space by performing a singular value decomposition along the lines suggested in Ref. [90].

For each set of testing parameters, we perform a separate LALINFERENCe analysis, where in concert with the full set of GR parameters [3] we also explore the posterior distributions for the specified set of testing parameters. Since our testing parameters are purely phenomenological (except the parameters that govern the PN early-inspiral stage), we choose their prior probability distributions to be uniform and wide enough to encompass the full posterior probability density function in the single-parameter case. In particular we set $\delta\hat{\varphi}_i \in [-20, 20]$; $\delta\hat{\beta}_i \in [-3, 3]$; $\delta\hat{\alpha}_i \in [-5, 5]$. In all cases we obtain estimates of the physical parameters – e.g., masses and spins – that are in agreement with those reported in Ref. [3].

In Fig. 6 we show the 90% upper bounds on the deviations in the (known) PN parameters, $\delta\hat{\varphi}_i$ with $i = 0, \dots, 7$ (except for $i = 5$, which is degenerate with the reference phase), when varying the testing parameters one at the time, keeping the other parameters fixed to the GR value. As an illustration, following Ref. [88], we also show in Fig. 6 the bounds obtained from the measured orbital-period derivative \dot{P}_{orb} of the double pulsar J0737-3039 [12]. Also for the latter, bounds are computed by allowing for possible violations of GR at different powers of frequency, one at a time. Not surprisingly, since in binary pulsars the orbital period changes at essentially a constant rate, the corresponding bounds quickly become rather loose as the PN order is increased. As a consequence, the double-pulsar bounds are significantly less informative than GW150914, except at 0PN order, where the double-pulsar bound is better thanks to the long observation time (~ 10 years against ~ 0.4 s for GW150914).⁶ Thus, GW150914 allows us for the first time to constrain the coefficients in the PN series of the phasing up to 3.5PN order.

Furthermore, in Table I and Fig. 7 we summarize the constraints on each testing parameter $\delta\hat{\varphi}_i$ for the single and multiple-parameter analyses. In particular, in the 6th and 7th columns of Table I we list the quantile at which the GR value of zero is found within the marginalized one-dimensional posterior (i.e., the integral of the posterior from the lower bound

⁶ We note that when computing the upper bounds with the binary-pulsar observations, we include the effect of eccentricity only in the 0PN parameter. For the higher PN parameters, the effect is not essential considering that the bounds are not very tight.

TABLE I. Summary of results for the gIMR parameterized-deviation analysis of GW150914. For each parameter in the gIMR model, we report its frequency dependence, its median and 90% credible intervals, the quantile of the GR value of 0 in the 1D posterior probability density function. Finally, the last two columns show \log_{10} Bayes factors between GR and the gIMR model. The uncertainties on the log Bayes factors are 2σ . The a and b coefficients shown for $\delta\hat{\alpha}_4$ are functions of the component masses and spins (see Ref. [41]). For each field, we report the corresponding quantities for both the single-parameter and multiple-parameter analyses.

waveform regime	parameter	f -dependence	median		GR quantile		$\log_{10} B_{\text{model}}^{\text{GR}}$	
			single	multiple	single	multiple	single	multiple
early-inspiral regime	$\delta\hat{\phi}_0$	$f^{-5/3}$	$-0.1^{+0.1}_{-0.1}$	$1.4^{+3.3}_{-3.0}$	0.94	0.21	1.9 ± 0.1	
	$\delta\hat{\phi}_1$	$f^{-4/3}$	$0.3^{+0.4}_{-0.4}$	$-0.4^{+0.7}_{-0.7}$	0.14	0.87	1.6 ± 0.1	
	$\delta\hat{\phi}_2$	f^{-1}	$-0.35^{+0.3}_{-0.35}$	$-3.2^{+19.3}_{-15.2}$	0.97	0.60	1.2 ± 0.2	
	$\delta\hat{\phi}_3$	$f^{-2/3}$	$0.2^{+0.2}_{-0.2}$	$2.6^{+13.8}_{-15.7}$	0.04	0.41	1.2 ± 0.1	
	$\delta\hat{\phi}_4$	$f^{-1/3}$	$-2.0^{+1.6}_{-1.8}$	$0.5^{+17.3}_{-18.2}$	0.98	0.49	0.3 ± 0.1	3.9 ± 0.1
	$\delta\hat{\phi}_{5l}$	$\log(f)$	$0.8^{+0.6}_{-0.55}$	$-1.5^{+19.1}_{-16.3}$	0.02	0.55	0.7 ± 0.1	
	$\delta\hat{\phi}_6$	$f^{1/3}$	$-1.5^{+1.1}_{-1.1}$	$-0.6^{+18.2}_{-17.2}$	0.99	0.53	0.4 ± 0.1	
	$\delta\hat{\phi}_{6l}$	$f^{1/3} \log(f)$	$8.9^{+6.8}_{-6.8}$	$-2.4^{+18.7}_{-15.2}$	0.02	0.57	-0.2 ± 0.1	
intermediate regime	$\delta\hat{\beta}_2$	$\log f$	$0.1^{+0.4}_{-0.3}$	$0.15^{+0.6}_{-0.5}$	0.29	0.35	1.2 ± 0.1	
	$\delta\hat{\beta}_3$	f^{-3}	$0.1^{+0.5}_{-0.3}$	$-0.0^{+0.8}_{-0.6}$	0.38	0.56	0.6 ± 0.1	2.2 ± 0.1
merger–ringdown regime	$\delta\hat{\alpha}_2$	f^{-1}	$-0.1^{+0.4}_{-0.4}$	$-0.0^{+1.0}_{-1.15}$	0.68	0.51	1.1 ± 0.1	
	$\delta\hat{\alpha}_3$	$f^{3/4}$	$-0.5^{+2.0}_{-1.5}$	$-0.0^{+4.4}_{-4.4}$	0.67	0.50	1.3 ± 0.1	2.1 ± 0.1
	$\delta\hat{\alpha}_4$	$\tan^{-1}(af + b)$	$-0.1^{+0.5}_{-0.6}$	$-0.0^{+1.2}_{-1.1}$	0.61	0.55	1.2 ± 0.1	

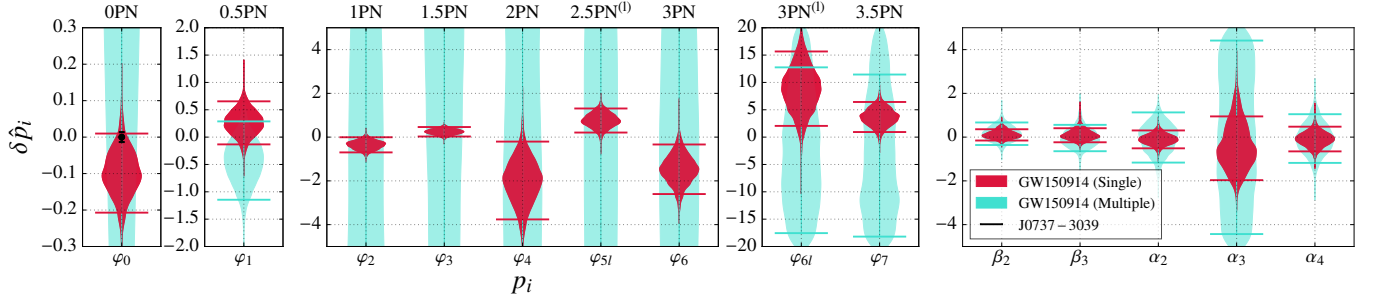


FIG. 7. Violin plot summarizing the posterior probability density distributions for all the parameters in the gIMR model. (Summary statistics are reported in Table I.) From left to right: the plot shows increasingly high-frequency regimes as outlined in the text and Fig. 3; the leftmost posteriors, labeled from 0PN to 3.5PN, are for the early-inspiral PN regime; the β_i and α_i parameters correspond to the intermediate and merger–ringdown regimes. Note that the constraints get tighter in the merger and ringdown regimes. In red, we show posterior probability distributions for the single-parameter analysis, while in cyan we show the posterior distribution for the multiple-parameter analysis. The black error bar at 0PN shows the bound inferred from the double pulsar; higher PN orders are not shown as their constraints are far weaker than GW150914’s measurement and they would appear in the plot as vertical black lines covering the entire y -axis. The 2.5PN term reported in the figure refers to the logarithmic term $\delta\hat{\phi}_{5l}$. Because of their very different scale compared to the rest of the parameters, the 0PN and 0.5PN posterior distributions from GW150914 and the double-pulsar limits at 0PN order are shown on separate panels. The error bars indicate the 90% credible regions reported in Table I. Due to correlations among parameters, the posterior distribution obtained from the multiple-parameter analyses in the early-inspiral regimes are informative only for the 0.5PN coefficient.

of the prior up to zero). We note that in the single-parameter analysis, for several parameters, the GR value is found at quantiles close to an equivalent of $2\text{--}2.5\sigma$, i.e., close to the tails of their posterior probability functions. It is not surprising that this should happen for the majority of the early-inspiral parameters since we find that these parameters have a substantial degree of correlation. Thus, if a particular noise realization causes the posterior distribution of one parameter to be off-centered with respect to zero, we expect that the poste-

riors of all the other parameters will also be off-centered. This is indeed what we observe. The medians of the early-inspiral single-parameter posteriors reported in Table I show opposite sign shifts that follow closely the sign pattern found in the PN series.

We repeated our single-parameter analysis on 20 datasets obtained by adding the same NR waveform with GW150914-like parameters to different noise-only data segments close to GW150914. In one instance, we observed $\delta\hat{\phi}_i$ posterior dis-

tributions very similar to those of Table I and Fig. 7, both in terms of their displacements from zero and of their widths, whereas for the others the displacements tended to be much smaller (though the widths were still comparable). Thus, it is not unlikely that instrumental noise fluctuations would cause the degree of apparent deviation from GR found to occur in the single-parameter quantiles for GW150914, even in the absence of an actual deviation from GR. However, we cannot fully exclude a systematic origin from inaccuracies or even missing physics in our waveform models. Future observations will shed light on this aspect.

In the multiple-parameter analysis, which accounts for correlations between parameters, the GR value is usually found to be very close to the median of the marginalized distributions. This is partly due to the fact that we are not sensitive to most of the early-inspiral parameters, with the exception of the 0PN and 0.5PN coefficients. As for the intermediate and merger-remnant parameters, since most of the SNR for GW150914 comes from the high-frequency portion of the observed signal, we find that the constraints on those coefficients are very robust and essentially independent of the analysis configuration chosen, single or multiple.

Finally, the last two columns of Table I report the logarithm of the ratio of the marginal likelihoods (the logarithm of the Bayes factor $\log_{10} B_{\text{model}}^{\text{GR}}$) as a measure of the relative goodness of fit between the IMRPhenom and gIMR models (see Ref. [3] and references therein). If $\log_{10} B_{\text{model}}^{\text{GR}} < 0 (> 0)$ then GR fits the data worse (better) than the competing model. The uncertainty over $\log_{10} B_{\text{model}}^{\text{GR}}$ is estimated by running several independent instances of LALINFEREN. The $\log_{10} B_{\text{model}}^{\text{GR}}$ values shown in Table I corroborate our finding that GW150914 provides no evidence in favor of the hypothesis that GR is violated.⁷

As an aside, we note that GW150914 was detected with the LIGO detectors at about one-third of their final design sensitivity, which is expected to be achieved around 2019 [19]. Hence future detections are expected to occur with larger SNRs, leading to tighter bounds on phase coefficients. It is also worth noting that the posterior density functions for the $\delta\hat{p}_i$ from all future detections can be combined, leading to a progressive improvement of the bounds on these parameters.

Constraining the graviton Compton wavelength. Since the 1970s, there have been attempts to construct theories of gravity mediated by a graviton with a non-zero mass. Those attempts have led to conceptual difficulties; some of these have been addressed, circumvented, or overcome, but others remain open (see Ref. [91] and references therein). Here, we

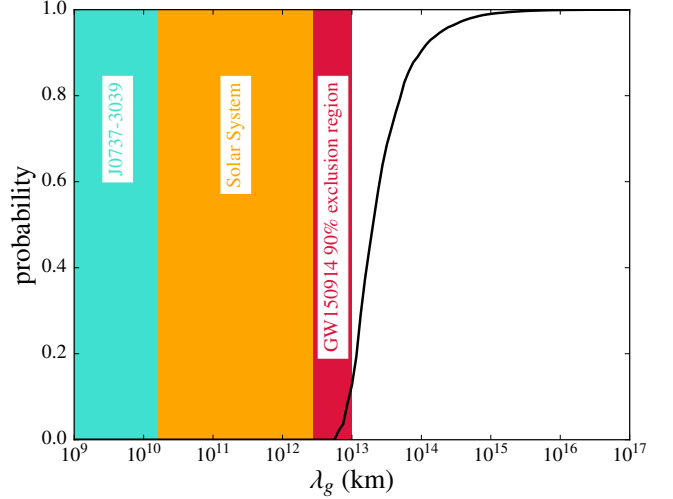


FIG. 8. Cumulative posterior probability distribution for λ_g (black curve) and exclusion regions for the graviton Compton wavelength λ_g from GW150914. The shaded areas show exclusion regions from the double pulsar observations (turquoise), the static Solar System bound (orange) and the 90% (crimson) region from GW150914.

take a phenomenological approach and consider a hypothetical massive-graviton theory in which, due to a modification of the dispersion relation, GWs travel at a speed different from the speed of light.

In GR, gravitons are massless and travel at the speed of light $v_g = c$. In a massive-graviton theory the dispersion relation can be modified to $E^2 = p^2 c^2 + m_g^2 c^4$, where E is the graviton energy, p the momentum, and m_g is the graviton rest mass, related to the graviton's Compton wavelength by $\lambda_g = h/(m_g c)$ with h the Planck constant. Thus, we have $v_g^2/c^2 \equiv c^2 p^2/E^2 \simeq 1 - h^2 c^2/(\lambda_g^2 E^2)$, and the massive graviton propagates at an energy (or frequency) dependent speed. Another effect one expects on general grounds is that the Newtonian potential gets altered by a Yukawa-type correction whose characteristic length scale is λ_g : $\varphi(r) = (GM/r)[1 - \exp(-r/\lambda_g)]$.

Existing bounds on λ_g that do not probe the propagation of gravitational interactions (i.e., the so-called *static* bounds), come from Solar System observations [92, 93] (which probe the above Yukawa-corrected Newtonian potential), the non-observation of superradiant instabilities in supermassive black holes [94], model-dependent studies of the large-scale dynamics of galactic clusters [95], and weak lensing observations [96]; these bounds are 2.8×10^{12} km, 2.5×10^{13} km, 6.2×10^{19} km and 1.8×10^{22} km, respectively. We note that the bound from superradiance relies on the assumption that the very massive, compact objects in the centers of galaxies are indeed supermassive Kerr black holes, as opposed to other, more exotic objects. As also stressed in Ref. [93], the model-dependent bounds from clusters and weak lensing should be taken with caution, in view of the uncertainties on the amount of dark matter in the Universe and its spatial distribution. The only *dynamical* bound to date comes from binary-pulsar ob-

⁷ Because of the normalization of the prior probability distributions, the Bayes factors include a penalty factor – the so-called Occam factor – for models that have more parameters. The wider the prior range for the additional parameters, the more severe the penalization. Therefore, different choices for $\delta\hat{p}_i$ would lead to different numerical values of $\log_{10} B_{\text{model}}^{\text{GR}}$. To fully establish the significance of the Bayes factors, validation studies [86, 87] would be necessary and will be presented in forthcoming studies.

servations [97] and it is $\lambda_g > 1.6 \times 10^{10}$ km. If the Compton wavelength of gravitons is finite, then lower frequencies propagate slower compared to higher frequencies, and this dispersion of the waves can be incorporated in the gravitational phasing from a coalescing binary. In particular, neglecting all possible effects on the binary dynamics that could be introduced by the massive graviton theory, Ref. [93] found that the phase term $\Phi_{\text{MG}}(f) = -(\pi Dc)/[\lambda_g^2(1+z)f]$ (formally a 1PN order term) should be added to the overall GW phase. In this expression, z is the cosmological redshift and D is a cosmological distance defined in Eq. (2.5) of Ref. [93].

GW150914 allows us to search for evidence of dispersion as the signal propagated toward the Earth. We perform the analysis by explicitly including the formally 1PN-order term above [93, 98] in the EOBNR and IMRPHENOM GW phases and treating λ_g as an additional, independent parameter [99]. We assume a standard Λ CDM cosmology [100] and a uniform prior probability on the graviton mass $m_g \in [10^{-26}, 10^{-16}]$ eV/c², thus the prior on λ_g is $\propto 1/\lambda_g^2$. In Fig. 8 we show the cumulative posterior probability distribution for λ_g obtained from combining the results of the two waveform models (EOBNR and IMRPHENOM) following the procedure outlined in Ref. [3]. We find no evidence for a finite value of λ_g , and we derive a dynamical lower bound $\lambda_g > 10^{13}$ km at 90% confidence, which corresponds to a graviton mass $m_g \leq 1.2 \times 10^{-22}$ eV/c². This bound is approximately a factor of three better than the current Solar-System bound [92, 93], and \sim three orders of magnitude better than the bound from binary-pulsar observations [97], but it is less constraining than model-dependent bounds coming from the large-scale dynamics of galactic clusters [95], weak gravitational-lensing observations [96], and the non-observation of superradiant instability in supermassive black holes [94].

No constraint on non-GR polarization states. GR predicts the existence of two transverse-traceless tensor polarizations for GWs. More general metric theories of gravitation allow for up to four additional polarization states: a transverse scalar mode and three longitudinal modes [13, 101]. Because the Hanford and Livingston LIGO instruments have similar orientations, they are sensitive to a very similar linear combination of the GW polarizations, so it is difficult to distinguish between the GR and non-GR states.

As an illustration, we use the BAYESWAVE GW-transient analysis algorithm [54] to reconstruct the GW150914 waveform, assuming the simplest case in which the signal consists entirely of the transverse scalar (breathing) mode. We compare the reconstructed waveforms and power spectral densities (PSDs) for the pure scalar-mode and GR models, and find the log Bayes factor between the two hypotheses to be $\log B_{\text{scalar}}^{\text{GR}} = 1.3 \pm 0.5$ when using the PSD from the breathing mode analysis and $\log B_{\text{scalar}}^{\text{GR}} = -0.2 \pm 0.5$ when using the PSD from the GR analysis. In both cases the log Bayes factors do not significantly favor one model over the other. The only notable difference is in the reconstructed sky locations; the latter reflects the different response of the detector network to the tensor components compared to the purely scalar mode.

We reiterate that this test is only meant to illustrate the difficulty in distinguishing between GR and non-GR polarization states on the basis of GW150914 data alone. Furthermore, the results are not in contradiction with the comprehensive parameter estimation studies of GW150914 [3], which model only the transverse-traceless GR polarizations. Finally, we note that in the weakly dynamical regime, binary pulsars [12] do provide evidence in favor of GR, in that they would have a different decay rate if scalar radiation dominated. To directly study the polarization content of gravitational radiation from the strong-field dynamics, a larger network including detectors with different orientations, such as Advanced Virgo [102], KAGRA [103], or LIGO-India [104] will be required, at least in the context of unmodeled GW-signal reconstruction.

Outlook. The observation of GW150914 has given us the opportunity to perform quantitative tests of the genuinely strong-field dynamics of GR. We investigated the nature of GW150914 by performing a series of tests devised to detect inconsistencies with the predictions of GR. With the exception of the graviton Compton wavelength and the test for the presence of a non-GR polarization, we did not perform any study aimed at constraining parameters that might arise from specific alternative theories [13, 14, 89], such as Einstein-æther theory [105] and dynamical Chern-Simons [106], or from compact-object binaries composed of exotic objects such as boson stars [107] or gravastars [108]. Studies of this kind are not possible yet, since we lack predictions for what the inspiral-merger-ringdown GW signal should look like in those cases. We hope that the observation of GW150914 will boost the development of such models in the near future.

In future work we will also attempt to measure more than one damped sinusoid from the data after GW150914's peak, thus extracting the QNMs and inferring the final black hole's mass and spin. We will, thus, be able to test the no-hair theorem [69, 70] and the second law of black-hole dynamics [73, 74]. However, signals louder than GW150914 might be needed to achieve these goals. GR predicts the existence of only two transverse polarizations for GWs. We plan to investigate whether an extended detector network will allow the measurement of non-transverse components [13] in further GW signals.

The constraints provided by GW150914 on deviations from GR are unprecedented due to the nature of the source, but they do not reach high precision for some types of deviation, particularly those affecting the inspiral regime. A much higher SNR and longer signals are necessary for more stringent tests. However, it is not clear up to which SNR our parameterized waveform models are still a faithful representation of solutions of Einstein's equations. Furthermore, to extract specific physical effects we need waveform models that are expressed in terms of relevant parameters. We hope that, encouraged by GW150914, further efforts will be made to develop reliable, physically relevant, and computationally fast waveform models. More stringent bounds can be obtained by combining results from multiple GW observations [61, 86, 87, 99]. Given the rate of coalescence of binary black holes as inferred

in Ref. [109], we are looking forward to the upcoming joint observing runs of LIGO and Virgo.

The detection of GW150914 ushers in a new era in the field of experimental tests of GR. The first result of this era is that, within the limits set by our sensitivity, all the tests performed on GW150914 provided no evidence for disagreement with the predictions of GR.

Acknowledgments. The authors gratefully acknowledge the support of the United States National Science Foundation (NSF) for the construction and operation of the LIGO Laboratory and Advanced LIGO as well as the Science and Technology Facilities Council (STFC) of the United Kingdom, the Max-Planck-Society (MPS), and the State of Niedersachsen/Germany for support of the construction of Advanced LIGO and construction and operation of the GEO600 detector. Additional support for Advanced LIGO was provided by the Australian Research Council. The authors gratefully acknowledge the Italian Istituto Nazionale di Fisica Nucleare (INFN), the French Centre National de la Recherche Scientifique (CNRS) and the Foundation for Fundamental Research on Matter supported by the Netherlands Organisation for Scientific Research, for the construction and operation of the Virgo detector and the creation and support of the EGO consortium. The authors also gratefully acknowledge research support from these agencies as well as by the Council of Scientific and Industrial Research of India, Department of Science and Technology, India, Science & Engineering Research Board (SERB), India, Ministry of Human Resource Development, India, the Spanish Ministerio de Economía y Competitividad, the Conselleria d'Economia i Competitivitat and Conselleria d'Educació, Cultura i Universitats of the Govern de les Illes Balears, the National Science Centre of Poland, the European Commission, the Royal Society, the Scottish Funding Council, the Scottish Universities Physics Alliance, the Hungarian Scientific Research Fund (OTKA), the Lyon Institute of Origins (LIO), the National Research Foundation of Korea, Industry Canada and the Province of Ontario through the Ministry of Economic Development and Innovation, the Natural Science and Engineering Research Council Canada, Canadian Institute for Advanced Research, the Brazilian Ministry of Science, Technology, and Innovation, Russian Foundation for Basic Research, the Leverhulme Trust, the Research Corporation, Ministry of Science and Technology (MOST), Taiwan and the Kavli Foundation. The authors gratefully acknowledge the support of the NSF, STFC, MPS, INFN, CNRS and the State of Niedersachsen/Germany for provision of computational resources.

Finally, we thank the anonymous referees, whose comments helped improve the clarity of the paper.

[1] B. P. Abbott et al. (LIGO Scientific Collaboration, Virgo Collaboration), *Phys. Rev. Lett.* **116**, 061102 (2016), <https://dcc.ligo.org/LIGO-P150914/public/main>.

- [2] B. P. Abbott et al. (LIGO Scientific Collaboration, Virgo Collaboration) (2016), <https://dcc.ligo.org/LIGO-P1500269/public/main>.
- [3] B. P. Abbott et al. (LIGO Scientific Collaboration, Virgo Collaboration) (2016), <https://dcc.ligo.org/LIGO-P1500218/public/main>.
- [4] J. Kepler, *Astronomia nova ..., seu physica coelestis, tradita commentariis de motibus stellae martis* (1609).
- [5] I. Newton, *Philosophiae Naturalis Principia Mathematica* (1687).
- [6] A. Einstein, *Preuss. Akad. Wiss. Berlin* p. 688 (1916).
- [7] A. Einstein, *Preuss. Akad. Wiss. Berlin* p. 154 (1918).
- [8] R. A. Hulse and J. H. Taylor, *Astrophys. J. Lett.* **195**, L51 (1975).
- [9] J. H. Taylor and J. M. Weisberg, *Astrophys. J.* **253**, 908 (1982).
- [10] L. Blanchet, *Living Rev. Rel.* **17**, 2 (2014).
- [11] M. Burgay et al., *Nature* **426**, 531 (2003).
- [12] N. Wex (2014), arXiv:1402.5594.
- [13] C. M. Will, *Living Rev. Rel.* **17**, 4 (2014).
- [14] E. Berti et al., *Class. Quant. Grav.* **32**, 243001 (2015).
- [15] T. Damour and G. Esposito-Farese, *Class. Quant. Grav.* **9**, 2093 (1992).
- [16] P. C. C. Freire et al., *Mon. Not. Roy. Astron. Soc.* **423**, 3328 (2012).
- [17] K. Schwarzschild, *Sitzungsber. Preuss. Akad. Wiss. Berlin (Math. Phys.)* **1916**, 189 (1916).
- [18] R. P. Kerr, *Phys. Rev. Lett.* **11**, 237 (1963).
- [19] J. Aasi et al. (LIGO Scientific Collaboration, Virgo Collaboration) (2013).
- [20] A. Buonanno and T. Damour, *Phys. Rev. D* **59**, 084006 (1999).
- [21] A. Buonanno and T. Damour, *Phys. Rev. D* **62**, 064015 (2000).
- [22] T. Damour, P. Jaranowski, and G. Schaefer, *Phys. Rev. D* **78**, 024009 (2008).
- [23] T. Damour and A. Nagar, *Phys. Rev. D* **79**, 081503 (2009).
- [24] E. Barausse and A. Buonanno, *Phys. Rev. D* **81**, 084024 (2010).
- [25] F. Pretorius, *Phys. Rev. Lett.* **95**, 121101 (2005).
- [26] M. Campanelli, C. O. Lousto, P. Marronetti, and Y. Zlochower, *Phys. Rev. Lett.* **96**, 111101 (2006).
- [27] J. G. Baker, J. Centrella, D.-I. Choi, M. Koppitz, and J. van Meter, *Phys. Rev. Lett.* **96**, 111102 (2006).
- [28] C. V. Vishveshwara, *Nature* **227**, 936 (1970).
- [29] W. H. Press, *Astrophys. J.* **170**, L105 (1971).
- [30] S. Chandrasekhar and S. L. Detweiler, *Proc. Roy. Soc. Lond. A* **344**, 441 (1975).
- [31] Y. Pan, A. Buonanno, J. G. Baker, J. Centrella, B. J. Kelly, S. T. McWilliams, F. Pretorius, and J. R. van Meter, *Phys. Rev. D* **77**, 024014 (2008).
- [32] P. Ajith et al., *Phys. Rev. D* **77**, 104017 (2008), [Erratum: *Phys. Rev. D* **79**, 129901 (2009)].
- [33] P. Ajith et al., *Phys. Rev. Lett.* **106**, 241101 (2011).
- [34] L. Santamaria et al., *Phys. Rev. D* **82**, 064016 (2010).
- [35] A. Taracchini et al., *Phys. Rev. D* **89**, 061502 (2014).
- [36] A. H. Mroué et al., *Phys. Rev. Lett.* **111**, 241104 (2013).
- [37] S. E. Field, C. R. Galley, J. S. Hesthaven, J. Kaye, and M. Tiglio, *Physical Review X* **4**, 031006 (2014).
- [38] M. Pürrer, *Class. Quant. Grav.* **31**, 195010 (2014).
- [39] M. Pürrer (2015), arXiv:1512.02248.
- [40] S. Husa, S. Khan, M. Hannam, M. Pürrer, F. Ohme, X. J. Forteza, and A. Bohé (2015), arXiv:1508.07250.
- [41] S. Khan, S. Husa, M. Hannam, F. Ohme, M. Pürrer, X. J. Forteza, and A. Bohé (2015), arXiv:1508.07253.
- [42] M. Hannam, P. Schmidt, A. Bohé, L. Haegel, S. Husa, F. Ohme, G. Pratten, and M. Pürrer, *Phys. Rev. Lett.* **113**,

151101 (2014).

[43] P. Kumar, T. Chu, H. Fong, H. P. Pfeiffer, M. Boyle, D. A. Hemberger, L. E. Kidder, M. A. Scheel, and B. Szilágyi (2016), arXiv:1601.05396.

[44] B. P. Abbott et al. (2016), <https://dcc.ligo.org/P1500259/public/main>.

[45] B. Bruegmann, J. A. Gonzalez, M. Hannam, S. Husa, U. Sperhake, and W. Tichy, Phys. Rev. **D77**, 024027 (2008).

[46] R. O’Shaughnessy, L. London, J. Healy, and D. Shoemaker, Phys. Rev. **D87**, 044038 (2013).

[47] M. A. Scheel, M. Giesler, D. A. Hemberger, G. Lovelace, K. Kuper, M. Boyle, B. Szilágyi, and L. E. Kidder, Class. Quant. Grav. **32**, 105009 (2015).

[48] T. Chu, H. Fong, P. Kumar, H. P. Pfeiffer, M. Boyle, D. A. Hemberger, L. E. Kidder, M. A. Scheel, and B. Szilágyi (2015), arXiv:1512.06800.

[49] C. O. Lousto, J. Healy, and H. Nakano (2015), arXiv:1506.04768.

[50] B. Szilágyi, J. Blackman, A. Buonanno, A. Taracchini, H. P. Pfeiffer, M. A. Scheel, T. Chu, L. E. Kidder, and Y. Pan, Phys. Rev. Lett. **115**, 031102 (2015).

[51] P. Schmidt, I. Harry, and H. Pfeiffer (2016), <https://dcc.ligo.org/LIGO-T1500606/public/main>.

[52] B. P. Abbott et al. (LIGO Scientific Collaboration, Virgo Collaboration) (2016), <https://dcc.ligo.org/LIGO-P1500229/public/main>.

[53] J. Veitch et al., Phys. Rev. **D91**, 042003 (2015).

[54] N. J. Cornish and T. B. Littenberg, Class. Quant. Grav. **32**, 135012 (2015).

[55] M. Vallisneri and N. Yunes, Phys. Rev. D **87**, 102002 (2013).

[56] S. Vitale and W. Del Pozzo, Phys. Rev. D **89**, 022002 (2014).

[57] T. A. Apostolatos, Phys. Rev. D **52**, 605 (1995).

[58] N. Cornish, L. Sampson, N. Yunes, and F. Pretorius, Phys. Rev. D **84**, 062003 (2011).

[59] M. Vallisneri, Phys. Rev. D **86**, 082001 (2012).

[60] J. Healy, C. O. Lousto, and Y. Zlochower, Phys. Rev. D **90**, 104004 (2014).

[61] A. Ghosh, A. Ghosh, N. K. Johnson-McDaniel, C. K. Mishra, P. Ajith, W. Del Pozzo, D. A. Nichols, Y. Chen, A. B. Nielsen, C. P. L. Berry, et al. (2016), 1602.02453.

[62] B. Allen, Phys. Rev. **D71**, 062001 (2005).

[63] Y. Pan, A. Buonanno, M. Boyle, L. T. Buchman, L. E. Kidder, H. P. Pfeiffer, and M. A. Scheel, Phys. Rev. **D84**, 124052 (2011).

[64] E. Berti, V. Cardoso, and C. M. Will, Phys. Rev. **D73**, 064030 (2006).

[65] O. Dreyer, B. J. Kelly, B. Krishnan, L. S. Finn, D. Garrison, and R. Lopez-Aleman, Class. Quant. Grav. **21**, 787 (2004).

[66] A. Buonanno, G. B. Cook, and F. Pretorius, Phys. Rev. D **75**, 124018 (2007).

[67] E. Berti, V. Cardoso, J. A. Gonzalez, U. Sperhake, M. Hannam, S. Husa, and B. Bruegmann, Phys. Rev. **D76**, 064034 (2007).

[68] I. Kamaretsos, M. Hannam, S. Husa and B. S. Sathyaprakash, Phys. Rev. D **85**, 024018 (2011).

[69] W. Israel, Phys. Rev. **164**, 1776 (1967).

[70] B. Carter, Phys. Rev. Lett. **26**, 331 (1971).

[71] S. Gossan, J. Veitch, and B. Sathyaprakash, Phys. Rev. D **85**, 124056 (2012).

[72] J. Meidam, M. Agathos, C. Van Den Broeck, J. Veitch, and B. S. Sathyaprakash, Phys. Rev. **D90**, 064009 (2014).

[73] S. W. Hawking, Phys. Rev. Lett. **26**, 1344 (1971).

[74] J. M. Bardeen, B. Carter, and S. W. Hawking, Commun. Math. Phys. **31**, 161 (1973).

[75] L. Blanchet and G. Schaefer, Class. Quant. Grav. **10**, 2699 (1993).

[76] L. Blanchet, Class. Quant. Grav. **15**, 113 (1998), [Erratum: Class. Quant. Grav. 22, 3381 (2005)].

[77] J. Lense and H. Thirring, Physikalische Zeitschrift **19**, 156 (1918).

[78] B. M. Barker and R. F. O’Connell, Phys. Rev. D **12**, 329 (1975).

[79] L. E. Kidder, Phys. Rev. **D52**, 821 (1995).

[80] L. Blanchet and B. S. Sathyaprakash, Classical and Quantum Gravity **11**, 2807 (1994).

[81] L. Blanchet, T. Damour, and B. R. Iyer, Phys. Rev. D **51**, 5360 (1995).

[82] L. Blanchet and B. S. Sathyaprakash, Phys. Rev. Lett. **74**, 1067 (1995).

[83] K. G. Arun, B. R. Iyer, M. S. S. Qusailah, and B. S. Sathyaprakash, Phys. Rev. D **74**, 024006 (2006).

[84] C. K. Mishra, K. Arun, B. R. Iyer, and B. Sathyaprakash, Phys. Rev. D **82**, 064010 (2010).

[85] N. Yunes and F. Pretorius, Phys. Rev. D **80**, 122003 (2009).

[86] T. Li, W. Del Pozzo, S. Vitale, C. Van Den Broeck, M. Agathos, et al., Phys. Rev. **D85**, 082003 (2012).

[87] M. Agathos, W. Del Pozzo, T. G. F. Li, C. Van Den Broeck, J. Veitch, and S. Vitale, Phys. Rev. D **89**, 082001 (2014).

[88] N. Yunes and S. A. Hughes, Phys. Rev. D **82**, 082002 (2010).

[89] N. Yunes and X. Siemens, Living Rev. Rel. **16**, 9 (2013).

[90] A. Pai and K. G. Arun, Class. Quant. Grav. **30**, 025011 (2013).

[91] C. de Rham, Living Rev. Rel. **17**, 7 (2014).

[92] C. Talmadge, J. P. Berthias, R. W. Hellings, and E. M. Standish, Phys. Rev. Lett. **61**, 1159 (1988).

[93] C. M. Will, Phys. Rev. D **57**, 2061 (1998).

[94] R. Brito, V. Cardoso, and P. Pani, Phys. Rev. **D88**, 023514 (2013).

[95] A. S. Goldhaber and M. M. Nieto, Phys. Rev. D **9**, 1119 (1974).

[96] S. R. Choudhury, G. C. Joshi, S. Mahajan, and B. H. J. McKellar, Astropart. Phys. **21**, 559 (2004).

[97] L. S. Finn and P. J. Sutton, Phys. Rev. **D65**, 044022 (2002).

[98] D. Keppel and P. Ajith, Phys. Rev. D **82**, 122001 (2010).

[99] W. Del Pozzo, J. Veitch, and A. Vecchio, Phys. Rev. D **83**, 082002 (2011).

[100] P. A. R. Ade et al. (Planck) (2015), arXiv:1502.01589.

[101] D. M. Eardley, D. L. Lee, A. P. Lightman, R. V. Wagoner, and C. M. Will, Phys. Rev. Lett. **30**, 884 (1973).

[102] F. Acernese et al. (Virgo), Class. Quant. Grav. **32**, 024001 (2015).

[103] Y. Aso et al. (KAGRA), Phys. Rev. **D88**, 043007 (2013).

[104] B. Iyer et al. (IndIGO Consortium) (2011), URL <https://dcc.ligo.org/LIGO-M1100296/public>.

[105] T. Jacobson and D. Mattingly, Phys. Rev. **D64**, 024028 (2001).

[106] S. Alexander and N. Yunes, Phys. Rept. **480**, 1 (2009).

[107] S. L. Liebling and C. Palenzuela, Living Rev. Rel. **15**, 6 (2012).

[108] P. O. Mazur and E. Mottola, Proc. Nat. Acad. Sci. **101**, 9545 (2004).

[109] B. P. Abbott et al. (LIGO Scientific Collaboration, Virgo Collaboration) (2016), <https://dcc.ligo.org/LIGO-P1500217/public/main>.